Solar Energy 201 (2020) 157–177

Contents lists available at ScienceDirect

Solar Energy

journal homepage: www.elsevier.com/locate/solener

Thermal analysis of a solar dryer equipped with PTSC and PCM using experimental and numerical methods

Zakaria Alimohammadi, Hadi Samimi Akhijahani*, Payman Salami

Department of Biosystems Engineering, Faculty of Agriculture, University of Kurdistan, Sanandaj, Iran

ARTICLE INFO

Keywords:
Apple slice
Drying efficiency
PCM
Thermal storage system
Working fluid

ABSTRACT

This paper was aimed to evaluate the effect of fluid type on thermal performance of parabolic trough solar collector (PTSC). The simulation process was performed to predict thermal variations in receiver tube and storage tank by CFD. The experiments were conducted with 0.025 kg/s as air flow rate. Four fluid types including Nano-fluid (Al_2O_3, 4%), engine oil (10W40), glycerin and water and were considered for the performance analysis. Moreover, the drying process of the solar dryer was considered during the drying of apple slices with 5 mm thickness. The results showed that overall input thermal energy for dryer was about 17.36 MJ, 18.46 MJ, 17.76 MJ and 16.80 MJ for Nano-fluid, oil, glycerin and water, respectively. It also implied that using Nanofluid, oil and glycerin improved the overall efficiency of the dryer about 9.7%, 20.2% and 12.4%, related to water. The comparison of simulated and predicted results it is implied that CFD method can predict the performance of PTSC with different working fluids with good accuracy. Using different working fluids assisted with PCM did not have undesired effect on the quality of dried apples.

1. Introduction

With growing the world population the energy demand for industrial and agricultural fields has increased as well. By the year 2100, about 90% of the energy consumed in the world must be supplied through renewable or new energy sources such as solar energy as a clean and abundant energy. More than 30% of produced world energy is consumed in agricultural fields which 3.6% is related to dry biological wet products (Trostle, 2008). The required energy was supplied by different types of fossil fuels and renewable energies. The literature review of energy sources shows that using renewable energy is very low compared to the fossil fuels and this leads to many environmental problems such as air pollution and global warming (Moloodpoor et al., 2019). On the other hand, the source of fossil fuels is limited and after some decades there will be no fossil fuel for the future (DanlamiMusa et al., 2018; Othman et al., 2017). Due to these reasons, application of equipments which used the renewable energy as a main source such as solar energy (a cleanness and abundance thermal energy source) could be a good solution to decrease the use of fossil fuels. Typically, solar collectors connected with thermal systems as a source of energy such as drying, heating and cooling systems. Dryers are the most used systems that produced thermal energy (from sources such as solar collectors) can be used for drying agricultural wet products. About 20–30% of energy demand in agricultural sector consumed for drying process which refers to remove the moisture content of wet products to increase the shelf life of agricultural products such as fruit. Also due to the remove the activation water the growth of microorganisms and corruption of the product significantly reduces (Aghbashlo et al., 2008). There are many dryers used in agricultural sectors and solar dryers due to use abundant solar energy are most popular. However some of the farmers use direct sun drying method to dry the products. Some factors such as dust, wind, insects, humidification at night and animal attack cause that the product dried via direct (open) sun drying method does not have proper quality. Consequently the quality of dried product could not be acceptable for the market and the price decreased significantly related to the other drying systems (Motahayyer et al., 2018). The comparison between the samples dried in solar dryer (SD) and open sun drying method (OSD) showed that profitability index for SD is above 1 in the year (Romano et al., 2009). The dried samples with two methods (traditional and solar drying) were studied in terms of microbial and sensory chemical properties. The results of chemical experiments showed that considering color characters, the samples dried with solar dryer were in better condition than the traditional method. There was no significant difference between two mentioned drying methods in term longevity which measured by HPLC chromatography. In the sensory evaluation, the dried solar samples were in a better condition than

* Corresponding author.
E-mail address: h.samimi@uok.ac.ir (H. Samimi Akhijahani).

https://doi.org/10.1016/j.solener.2020.02.079
Received 12 November 2019; Received in revised form 27 January 2020; Accepted 22 February 2020
Available online 05 March 2020
0038-092X/

Nomenclatures

A_a	collector surface (m^2)
A_e	radiation area (m^2)
A_{mush}	mushy zone constant (–)
A_r	receiver tube surface (m^2)
A_t	PCM container surface (m^2)
c_p	specific heat capacity of fluid (J/kg·K)
$c_{p,nf}$	specific heat of nanofluid (J/kg K)
d_f	base fluid diameter (m)
d_p	nano-particles diameter (m)
D_i	inner diameter of tube (mm)
DR	drying rate (kg water/kg dry matter·min)
D_{gi}	inner diameter of glass cover (m)
D_{go}	outer diameter of glass cover (mm)
D_{ri}	inner diameter of receiver tube (m)
D_{ro}	outer diameter of receiver tube (m)
E_{st}	energy stored in tank (J)
f	friction factor (–)
F_R	collector heat removal coefficient (–)
g	gravity acceleration (m/s^2)
G_b	turbulence kinetic energy Generated via buoyancy (J)
H	enthalpy (J/kg)
h_a	convection heat transfer coefficient of ambient air (W/m K)
h_f	convection heat transfer coefficient of fluid (W/m K)
h_t	convection heat transfer coefficient for fluid inside storage tank (W/m K)
k_f	fluid conductivity (W/m K)
k_g	thermal conductivity of glass (W/m K)
k_{nf}	thermal conductivity of nanofluid (W/m K)
k_r	thermal conductivity of receiver (W/m K)
k_w	thermal conductivity of copper (W/mK)
L	tube length (mm)
L_v	vaporization latent heat of moisture (kJ/kg)
M_e	equilibrium moisture content of the slices (kg water/kg dry matter)
M_f	final moisture content (kg water/kg dry matter)
M_o	initial moisture content (kg water/kg dry matter)
M_t	moisture content considered for slices at time (kg water/kg dry matter)
MR	moisture ratio (–)
m_{pcm}	mass of PCM (kg)
Nu	Nusselt number (–)
Pr	Prandtl number (–)
Q_f	energy flux of fluid in tank (J/s)
$Q_{in,dryer}$	input energy (thermal) to the drying system (J)
$Q_{out,dryer}$	output energy (thermal) of the dryer (J)
Q_s	available useful solar thermal energy (J)
P_{fan}	power consumed by Fan (W)
P_{pump}	power consumed by pump (W)
Re	Reynolds number (–)
$\vec{S}$	term for momentum (N/m)
S_k	additional source terms of k
S_ε	additional source terms of ε
t	time (s)
$T_{f,in}$	fluid temperature at inlet for tank (K)
$T_{f,out}$	outlet fluid temperature of tank (K)
$T_{f,,m}$	mean working fluid temperature (K)
$T_{w,m}$	mean tube wall temperature of paraffin (PCM) container (K)
T_{pcm}	PCM temperature(K)
t_w	wall thickness (mm)
T_1-T_2	temperature difference (K)
u	fluid velocity(m/s)
U_L	overall heat loss coefficient (W/m^2K)
$\vec{V}$	vector of velocity (m/s)
W_a	initial weight (kg)
α	absorption coefficient (–)
β	volumetric expansion coefficient of PCM (1/K)
ε_g	emittance of outer glass (–)
η	the energy efficiency of the collector (–)
η_{dryer}	drying efficiency (–)
θ	reflection coefficient (–)
μ	dynamic viscosity ($N·s/m^2$)
ρ_f	fluid density (kg/m^3)
ρ_p	nanoparticle Density (kg/m^3)
σ	Stefan-boltzmann constant ($W/m^2\ K^4$)
τ	diffusion coefficient (–)
ϕ	volumetric fraction of nanoprticle (–)
ΔP	pressure drop (Pa)

the traditional method and there was a significant difference between the solar and traditional dry samples ($p < 0.05$) (Javadi-Yanblagh and Toori-Bidgoli, 2015). Microbial test of samples showed that in terms of total and total counts, the dried samples were at standard level but the in traditional method dried samples were not within the standard range (Samimi-Akhijahani et al., 2016). According to the economic analysis carried out in other research the investment return rate is about 55%, which is higher than the maximum investment rate thus it can be claimed that this project is suitable for any investment. Based on these analyses, the plan has a one-year invest return period, which seems appropriate for raising whole capital (Ross et al., 2007). Thus considering quality factors and price of dried samples solar drying is suitable way for drying of the products with low change in quality and market price. Iran is one the countries that because of higher radiation intensity (4.45 $kWhm^2$/day) and higher sunny days (about 280 days in a year) solar dryers are mostly developed and constructed (Motahayyer et al., 2018). Kurdistan province located at west of Iran and Sanandaj city with higher solar radiation intensity and radiation times (about 9.5 h per day during a year) is a proper region for solar drying. However, due to the lower thermal efficiency, the solar dryers are less considered for thermal usage (Arabhosseini et al., 2019) and people would like to use other system. Therefore, much effort such as combining system, using phase change materials, application of heat pump system and using fluid with higher heat capacity have been done for improving the performance of the solar dryers. By using the mentioned methods it was predicted that solar energy production was increased about 8.9% annually between 2012 and 2040 all over the world (Khosravi et al., 2019).

Proper design and construction of the collectors is an important factor to use renewable energies especially solar energy. Solar collectors are the most used thermal systems to convert solar radiation to thermal energy and the produced energy consumed in solar dryers. Among the solar collectors which connected to the storage system, Parabolic Trough Solar Collectors (PTSC) with higher thermal performance and lower maintenance and installation cost are more efficient (Yilmaz and Soylemez, 2014). PTSC due to have a proper performance through whole year even when the solar radiation is low, the use of sun tracking system, operating in medium to higher outlet temperature, using different types of working fluids and hybridizing with other systems are most used in thermal systems (Yaghoubi et al., 2013; Mohammad zadeh et al., 2015; Khosravi et al., 2019; Habibi et al., 2019). Various studies have been performed to heat transfer analysis and increase the efficiency of PTSC. In a study the detailed thermal model of the receiver of PTSC was investigated (Kalogirou, 2012). The effect of using vacuum

shell around the receiver tube was studied and the improving thermal performance of the collectors was resulted (Daniel et al., 2011). Thermal performance of a PTSC was investigated via a swarm intelligence optimizer. The tube was modeled in one dimensional form and the results indicated that the model can predict the performance of the thermal system with good accuracy (Moloodpoor et al., 2019). Bellos et al. (2018) investigated the use of multiple cylindrical longitudinal inserts in PTSC on the performance of collector with 15 different cases. They found that using four inserts increase the heat transfer coefficient about 26.88% (Bellos et al., 2018). In a research ferrofluid materials were applied to improve heat transfer of the working fluid. Moreover, the effect of magnetic field was analyzed and the results showed that it increases the collector performance (Khosravi et al., 2019). The performance of a PTSC (considering heat transfer) was improved using nanofluids as the working fluid inside the collector (Malvandi et al., 2016; Kasaeian et al., 2015). The thermal efficiency of a PTSC was investigated using three various working fluids: oil, pressurized water and oil mixed by nanoparticles. The results indicated that using nanofluids increased the thermal efficiency about 4.25% (Bellos et al., 2016a). Ghasemi et al. (2013) studied the influence of using Al_2O_3-Therminol 66 and Al_2O_3-water nanofluids on the performance of PTSC. They used CFD simulation for analyzing the thermal system and the results revealed that nanofluids improves the heat transfer of the collector. In a study the thermal performance of a PTSC considering useful exergy, mass flow rate, heat removal factor and the ratio of concentration was theoretically investigated (Manikandan et al., 2012). Gas working fluids were used in a PTSC and energetic and exergetic analysis was carried out (Bellos et al., 2016b).

The low efficiency of PTSC could be improved using fluids with higher heat capacity, higher thermal conductivity and storing thermal energy inside the storage tank. In the other words working fluid is the important part of PTSC. Use of the inappropriate working fluid reduces absorbed thermal energy (Neha, 2012) and consequently decreases the thermal efficiency or performance of the system attached with the collector such as solar cabinet dryer. In the other hand by using thermal storage system (tank, fluid and phase change materials) the rate of energy storage increases when the solar radiation rises through the experimental days. There are some materials (fluid or fluid + solid) used in Parabolic Trough Solar Collectors such as hydraulic oil (Abbood and Mohammed, 2019), CeO_2/water (Sharafeldin and Grof, 2018), Al_2O_3 (Bellos and Tzivanidis, 2017), Al_2O_3/synthetic oil nanofluid (Sokhansefat et al., 2014), CuO (Mwesigye et al., 2015), Syltherm800/Al_2O_3 (Mwesigye and Huan, 2015) oil/Al_2O_3 (Wang et al., 2016) Cu-water (Ghasemi and Ranjbar, 2016), Fe_3O_4-water (Khosravi and Malekan, 2018) and TiO_2 (Toghyani et al., 2016). Most of the mentioned working fluid increases the performance of the collector related to water. Moreover computational fluid dynamics as a suitable, powerful and accurate software for thermal design in industrial uses and fluid dynamics can be used to analyze and optimize the thermal systems (Darabi et al., 2013; Boulard and Wang, 2002). Considering this fact that the geometrical design of the collector and the type of fluid flows inside the system are directly affected on the thermal performance of PTSC, experimental validation of the system at different condition is very difficult and time consuming (Ghasemi and Ranjbar, 2016; Panchal Ramchandra and Bhosale, 2016; Dutil et al., 2011). Thus using CFD method increases the accuracy of the project and decreases the cost and the time used for thermal analysis of the system. Several studies can be found in the literature that investigated the effect of using different fluids on heat transfer and the thermal performance of parabolic trough collectors via CFD method.

Numerical analysis of PTSC was investigated via CFD method using magnetic field and ferrofluids. The results illustrated that using magnetic field improved receiver tube heat transfer coefficient and thermal efficiency (performance) of PTSC (Khosravi and Malekan, 2018). In the other paper the convective heat transfer of a nanofluid (Al_2O_3/synthetic 800) was simulated using CFD method. Two-phase model was considered for simulation process and the results indicated that for the working fluid with 4% volume fraction, the relative error for collector efficiency and outlet temperature was about 10% and 0.3%, respectively (Kaloudis et al., 2016). Thermal efficiency of PTSC with Al_2O_3-water and Al_2O_3-Therminol 66 nanofluids was studied via CFD simulations. The results demonstrated that using bigger nanoparticle with higher volume fraction of nanofluids increases Nusselt number. Moreover using nanofluids improved the collector heat transfer coefficient (Ghasemi and Ranjbar, 2016). Dynamic behavior of a direct steam using PTSC was evaluated by experimental CFD simulation method. The simulated data shows a good agreement with the experimental obtained data by variation of solar radiation (Lobon et al., 2014). Three dimensional analysis of PTSC in a solar power plant was performed using CFD analysis in COMSOL Multi-physics software. The results showed that due to non-homogenous solar radiation the temperature of cover surface of the tube has lower temperature related to the other sections (Marrakchi et al., 2018). Hachicha et al. investigated 3D CFD simulation model of PTSC based on Large Eddy Simulation (LES). Instantaneous velocity and pressure diagrams compared for different pitch angles and wind velocity. The results showed the similar trends of Nusselt number for the ambient air velocity with higher and lower levels (Hachicha et al., 2014). In a study genetic algorithm (GA) and CFD methods was used to optimize thermal efficiency of PTSC. It was found that porous disk with steam improved up to 3% (Zheng et al., 2016). Munoz and Abanades proposed a set of finned tube configurations that reduced thermal losses and fluid temperature in the tube. The analysis was performed using CFD simulation method and about 3% improvement of the collector was resulted (Munoz and Abanades, 2011). Moreover other studies used CFD simulation method to analyze the heat transfer process and optimize the solar system such as application of CFD method to simulate the solar agricultural dryer with or without thermal storage system (Amjad et al., 2015; Tarigan, 2018, Krawczyk and Badyda, 2011; Demissie et al., 2019). The results of the storage system investigations illustrated that to obtain the better thermal efficiency of the storage system the dimensional design, the conditions of the PCM (the location in the system and the amount), operating conditions and the validation of the system using experimental data is required (Dutil et al., 2011). The review of the investigation of CFD model as the simulation method to predict heat transfer in solar systems with PCM as storage unit illustrated that CFD models can be considered as an accurate prediction method related to the complicated mathematical models (Allouche et al., 2016; Al-abidi et al., 2013). In most engineering processes phase change materials were used such as: building thermal storage systems, cooling technology supported by electrical source and HVAC (heating, ventilation and air conditioning) and CFD method can properly predict the performance of the systems. The thermal behavior of the energy storage system considering PCM have been studies via CFD method: Allouche et al., 2016; Tay et al., 2012a,b; Trp et al., 2006; Gertzos and Caouris, 2007; Hosseini et al., 2012; Xiaohong et al., 2011. The results of the studies indicated CFD as a proper tool to simulate the thermal performance of storage system with PCM with a good correlation coefficient ($0.87 < R^2 < 0.98$).

According to the results of the studies in the literature it can be stated that because of the higher heat losses from the collectors the thermal efficiency of the dryers equipped by solar collectors is very low. This leads to less use of solar dryers in agricultural filed. Considerable amount of solar energy reflected to focal line, due to the inappropriate property of the working fluid it losses from the receiver tube or the storage tank. Using suitable fluid with PCM could be a proper way to solve the mentioned problem. This is very noticeable when the solar radiation intensity is at the higher level (around noon time). The working fluid absorbs more thermal energy imported to the storage tank, saves it in the working fluid flows in the system and specified weight of PCM and released it when the solar radiation is lower. Due to entering the air with homogenous temperature to the dryer the quality of dried product improved. Most of the quality characters of the dried

products decreases due to higher temperature entered to the dryer (Aghbashlo et al., 2008) especially when the solar radiation is high. By considering the literature review on PTSC there is little information on the thermal behavior of solar dryer equipped with PTSC and PCM via experimental and simulated methods. Thus in this paper the performance of a PTSC including inlet thermal energy and thermal efficiencies with four working fluids were investigated. The variations of heat transfer coefficient, heat transfer, thermal losses, thermal performance of the solar collector and the connected solar dryer were estimated at different conditions considering experimental and simulation methods. Moreover the effects of using different fluids on the drying kinetics and the quality of dried apple slices were studied. Due to high accuracy of Ansys – Fluent software, 3D model of the system was considered for any transient simulation. Therefore the system (including receiver and thermal storage system) was designed and developed and energy performance was investigated numerically. Meanwhile some apple slices considered to evaluate and describe the drying kinetic and drying performance of solar system. To illustrate the adverse effect of the solar system on the drying process, the quality of dried sample compared with the other system used for drying of apple samples. Finally the data obtained by CFD model verified considering the experimental data.

2. Materials and methods

2.1. Experimental set up

To do the experiments and survey the performance of the collector and solar dryer a PTSC equipped with a heat pipe constructed in renewable energy research centre of university of Kurdistan, Sannadaj, Iran. Due to the lower heat convection between the surfaces of the tube and the space it was considered vacuum. During the experimental days, solar radiation concentrated in to the absorbing tube by a parabolic concentrator. The tube was situated on the focal section of the parabolic

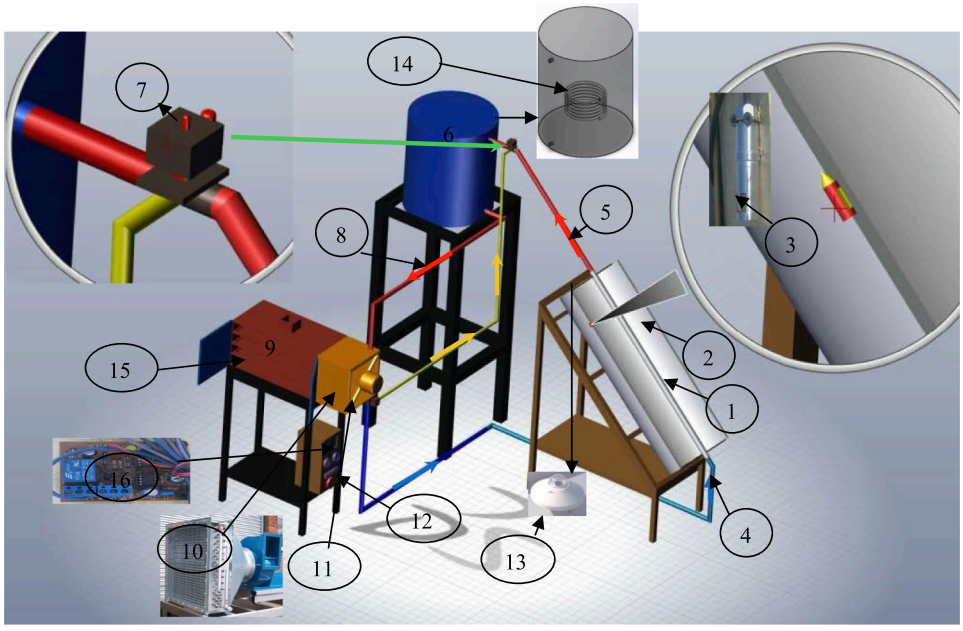

a

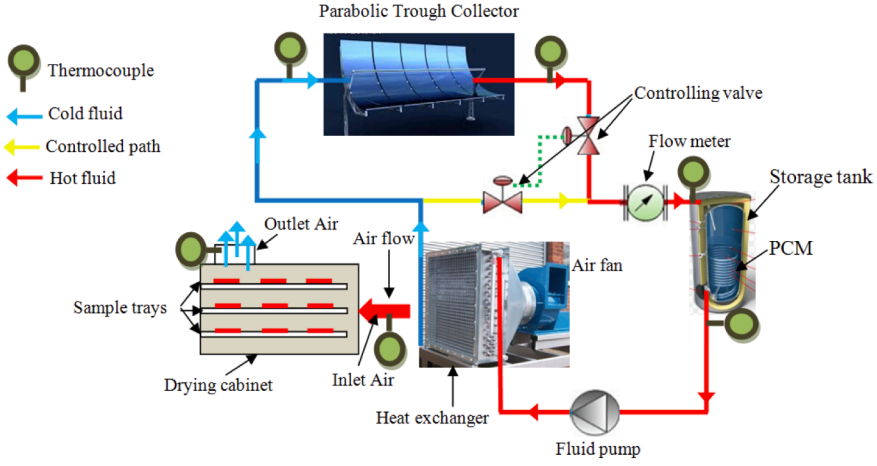

b

Fig 1. a. The pictorial view of solar dryer equipped with 1- receiver tube, 2- reflector, 3- sun tracking sensor, 4- cold fluid flow 5- hot fluid flow, 6- storage tank, 7- electric valve, 8- fluid flow from storage tank to heat exchanger, 9- cabinet, 10- heat exchanger, 11- fan, 12- data logger and temperature controller, 13- pyranometer, 14- PCM container tube, 15- sample trays, 16- sun tracking controller; b. The schematic of the drying system with working fluid and recycling system.

reflector. The working fluid flows to the collector passes through the absorbing tube and the thermal energy transmitted to the fluid. By variation the fluid the amount of heat absorbed by the collector varies as well (Khosravi et al., 2019). Considering the local concentration ratio of the absorber tube it shows that about half of the tube surface dose not receive the concentrated solar radiation which reflected by the parabolic plate. From the beginning of a day by increasing solar radiation the produced thermal energy absorbed by working fluid, moves through the receiver tube enters to the container and thermal energy stored by fluid and PCM in container (red arrows in Fig. 1a,b). Then the fluid flows toward the heat exchanger and by passing the air through pipes and fines of heat exchanger, the air heated, entered to the cabinet to dry samples as shown in Fig. 1b. The working fluid flows out of the heat exchanger and moves toward the receiver tube of PTSC. This operation continued until the intensity of solar radiation decreased. After that the electrical valve cuts the blue line and opens the yellow line to flow the fluid between the dryer and storage tank. In all the day time the collector chases the solar rays using sun tracking system (photocell sensor, electrical circuit and electrical motor). The main component with details of the dryer showed in Fig. 1.

Fluid as the main part of the dryer for heat transferring process was heated inside the receiver due, absorbs thermal energy from the sun. Then it moved via a DC pump with 4.2 l/min to the storage tank which has fluid and PCM. By the time the solar radiation intensity increase and fluid temperature in the fluid container increased as well. Due to have the storage system thermal energy for drying of apple slice can be provide for a while (especially at night time) and the drying continued. Table 1 illustrated the details of PTSC solar dryer.

2.2. Nanofluid preparation process

For using nano-particles in thermal systems some vital property are of interest to the researchers such as higher thermal conductivity (Kaya et al., 2019), good stability, lower weight and lower cost materials (Zhai et al., 2019). In this study Al_2O_3 was selected as nanoprticles which mixed in water as base fluid. The concentration of Al_2O_3 was about 4.0% and the size of the nano-particles was about 20 nm. The production sustainable or stable nano-fluid is a critical factor to estimate the effect of nanofluids on the thermal performance of solar collectors (Tong et al., 2019). To produce the stable nanofluid two step method was considered (Kaya et al., 2019): at step one the nanopaticles added to the base fluid mixed by a magnetic stirrer for about 10–15 min at 20 °C. Then the blend was placed in an ultrasonic homogenizer (UHP-400, Iran Ultrasonic) for about 5hr by a power of 50 W and frequency of 20 kHz. The dispersion stability of the nanaofluid was estimated using visual inspection test after an hour, 12 h, one day, three days and one week. As shown in Fig. 2, No significant change was absorbed for the mixtures after mentioned time intervals at room temperature.

2.3. Measuring tools

The temperature of selected points of the dryer, collector tube and storage tank was controlled by an automatic temperature controller (accuracy = ± 0.1 °C) and K type calibrated thermocouples and a data-logger (Model: DL-9601A, Lutron). The controlling unit recorded and saved the desired points temperature during the drying of samples. The environmental relative humidity was recorded every 30 min by a hygrometer with an accuracy of 0.1% (HT, 3600, Lutron, Taiwan). The ambient air relative humidity and air temperature was about 15.2–21.4% and 17–32.5 °C during the test days. For controlling the radiation intensity a pyranometer with the accuracy of ± 1 W/m^2 (TES-1333R, Taiwan) was installed to the system. The airflow at different points of the dryer was controlled by speed controller (model AM- 4206, Lutron, Taiwan). The flow rate of the working fluids was controlled using a flowmeter (PROMAG – 53P).

2.4. Mathematical Procedure

In present section the mathematical equations which used to evaluate PTSC are presented. Parabolic trough solar collectors are mainly contained of three parts: chassis, receiver tube and concentrator.

2.4.1. Thermal analysis of receiver tube

To calculate the thermal efficiency, heat flux and heat losses the thermal modeling and numerical analysis of PTSC is required. Therefore the system was modeled by linear thermal resistance method with nodal temperature points. The model was pictured in Fig. 3. Energy balance of equations per unit length of different parts of the system was considered. As shown in Fig. 3 the solar irradiation is received by glass cover and absorbed by outer surface of the absorber tube. A portion of absorbed thermal energy is transferred to inner surface of the tube via conduction mechanism. The thickness and heat transfer coefficient of the tube affected on this process. The thermal energy then transferred to the working fluid via convection process and the other part of absorbed energy transmitted to the inner surface of the glass cover via convection and radiation process. The thermal energy transferred to the inner surface of glass cover is conveyed to the outer surface via conduction process. Finally it is transferred to the environment via convection and radiation. For thermal modeling of PTSC, the steady state with constant heat flux condition was considered. In the other words, all the temperatures and thermal parameters are uniform around the receiver tube and the temperature fluctuation has not significant effects on thermal analysis. The heat transfer coefficient for receiver tube is defined according to the Nusselt number and the condition of flow inside the tube. Considering the flow in the pipe, the Reynolds number is higher than 2300, thus turbulent and transitional flow cases are happened in the receiver tube. Nusselt number can be estimated with Eq. (1) (Mwesigye et al., 2015):

Table 1
Description the details of PTSC and solar cabinet dryer assisted with PCM.

Components	Details
Receiver tube	A tube, with diameter of 30 mm, the length 2100 mm, thickness of1mm, covered by Al-Cu via black film with emittance of 0.08 and the absorptance of 0.93
Solar concentrator	A stainless steel with the reflection 0.88 and absorption of 0.1, the concentration factor of 25.
Transferring tube	PVC tubes insulated by glass wool
Storage tank	A circular tank, about 200 L, insulated by glasswool with 40 mm thick
Fluid circulator	Axial pump with maximum flow rate of 4.2 l/min, 12 V, 10 Ampere (NM, 32-60-180)
Heat Exchanger	Containing 68 rows, With 5 mm diameter, 10 mm distance between the rows thorough 320 mm × 400 mm, Model: Welo Armko, Made by koshesh radiator, Iran.
Solar dryer cabinet	A medium-density fiberboard (MDF) with 10 mm thick and dimensions of 1000 × 600 × 600 mm, insulated by glasswool with 40 mm thick, A rectangle wooden trays with dimensions of 900 mm × 500 mm
Air ventilator	A12 volt DC fan (Sunon, China)
PCM	A spiral copper tube with 1 mm thickness, 1000 mm length, 30 mm diameter and 6 turns

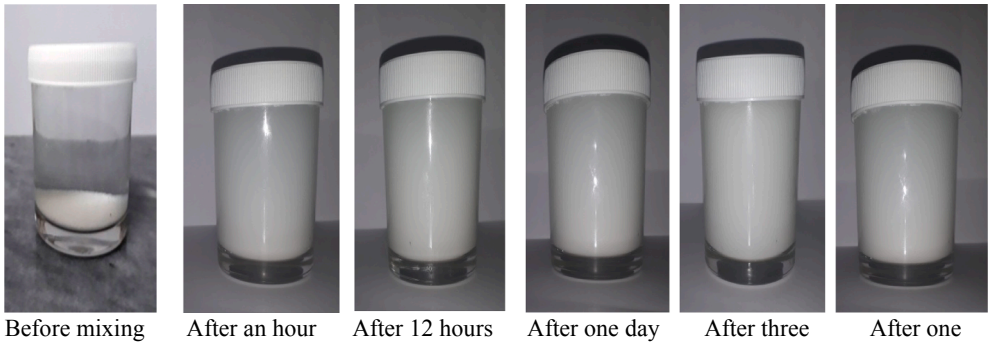

Fig. 2. Stability of the nanofluid solution after defined interval times.

$$Nu_x = \frac{f}{8}\frac{(Re-1000)Pr}{1+12.7\left(\frac{f}{8}\right)^{0.5}(Pr^{0.66}-1)} \quad (1)$$

where *Pr* and *Re* are Prandtl number and Reynolds number, respectively.

The friction factor (f) can be determined by Eq.2 considering pressure drop along the absorber tube (Bellos and Tzivanidis, 2017):

$$f = \frac{2\Delta P}{\rho_f u^2}\left(\frac{D_i}{L}\right) \text{ or } f = (0.79.\ \ln Re - 1.64)^2 \quad (2)$$

where ΔP represent the pressure drop, D_i the inner diameter of tube, L the tube length, ρ_f is fluid density and u the fluid velocity.

To calculate the thermal energy transfer between the receiver tube and working fluid the following equation was used (Moloodpoor et al., 2019; Duffie and Beckman, 2013):

$$\dot{Q}_{conv,1-2} = h_f \pi D_i (T_2 - T_1) \quad (3)$$

T_1 and T_2 are fluid and inner receiver tube temperature, respectively.

h_f represent convection heat transfer coefficient for the fluid which is dependent on the fluid thermal conductivity (k_f), inner diameter of receiver tube and Nusselt number can be obtained using Eq. (4):

$$h_f = Nu_f \frac{k_f}{D_i} \quad (4)$$

The heat conduction trough the receiver tube can be estimated using Eq. (5):

$$\dot{Q}_{cond,2-3} = \frac{2\pi k_r L(T_3 - T_2)}{\ln(\frac{D_{ro}}{D_{ri}})} \quad (5)$$

k_r is thermal conductivity of the receiver tube. It is mentioned that

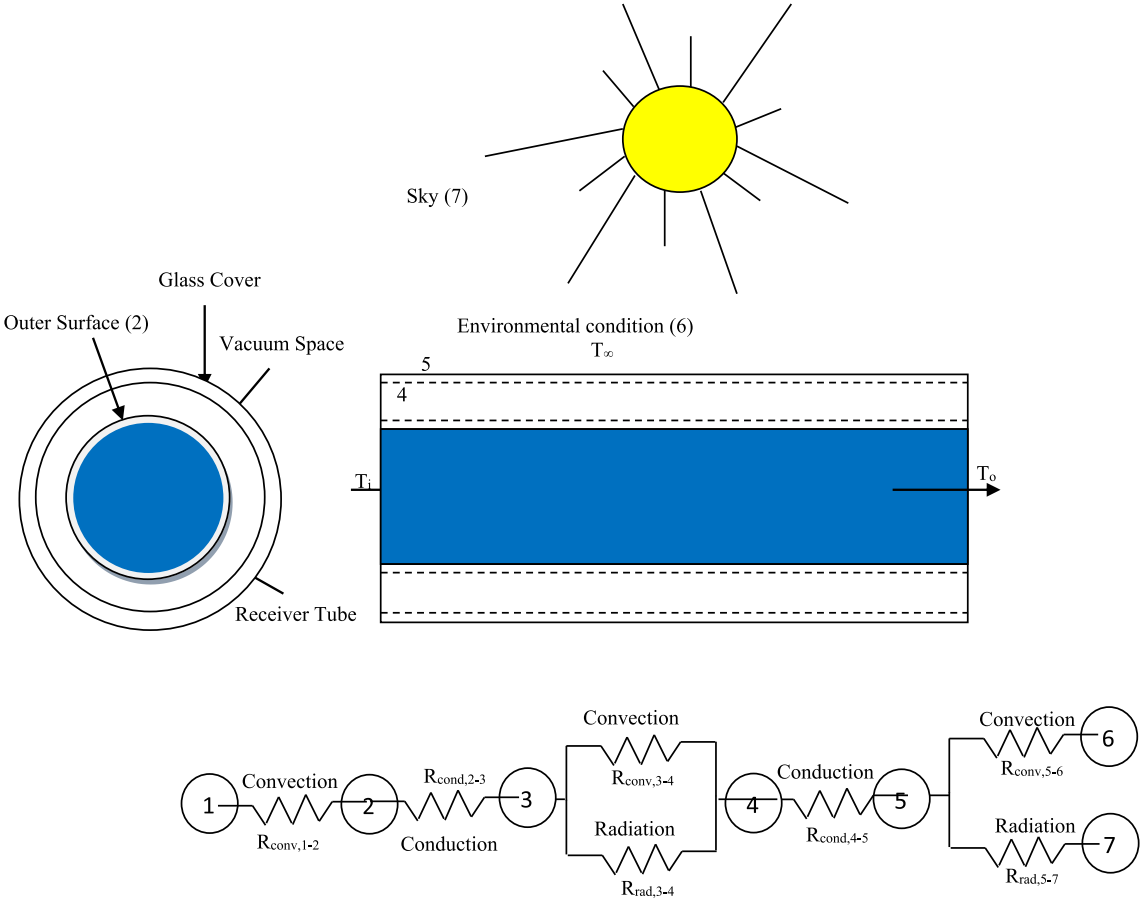

Fig. 3. Heat transfer and thermal resistance model of the receiver tube of PTSC.

in this study the thickness of receiver wall is very thin ($D_{ri} \approx D_{ro}$), thus the conduction process in this part is very low and it is neglected.

For the annular section of the receiver, the heat transfer occurred via convection Eq. (6) and radiation Eq. (7):

$$\dot{Q}_{conv,3-4} = \frac{2\pi k_{eff} L(T_4 - T_3)}{\ln(\frac{D_{gi}}{D_{ro}})} \quad (6)$$

$$\dot{Q}_{rad,3-4} = \frac{\pi D_{ro} L\sigma(T_3^4 - T_4^4)}{\frac{1}{\varepsilon_r} + \frac{1-\varepsilon_g}{\varepsilon_g}(\frac{D_{gi}}{D_{ro}})} \quad (7)$$

Due to vacuum space between points 3 and 4, there is no convective heat transfer (keff = 0), thus the value of the $\dot{Q}_{conv,3-4}$ in the Eq. (6) is not significant.

D_{gi} is inner diameter of glass cover, σ is Stefan Boltzmann constant (5.67×10^{-8} W/m^2 K), ε_r and ε_g are emissivity of receiver tube (0.12–0.13) and glass cover (0.86), respectively. k_{eff} is effective thermal conductivity which is depend on Prandtl and Reyleigh number (Duffie and Beckman, 2013).

Between the points 4 and 5 (for inner and outer surface of glass cover) the conduction mechanism occurred:

$$\dot{Q}_{cond,4-5} = \frac{2\pi k_g L(T_5 - T_4)}{\ln(\frac{D_{go}}{D_{gi}})} \quad (8)$$

k_g represents the glass cover thermal conductivity, D_{gi} and D_{go} are inner and outer diameter of glass cover.

The heat transfer for the glass cover and the environment was divided in two sections: convection between the glass and ambient and radiation between glass and sky:

$$\dot{Q}_{conve,5-6} = (\pi D_{go} L h_a(T_5 - T_6)),\ \dot{Q}_{rad,3-4} = (\pi\varepsilon_g D_{go} L h_g \sigma(T_5^4 - T_7^4)) \quad (9)$$

h_a referred to convected heat transfer coefficient of ambient air around the absorber tube (receiver). T_7 represents the sky temperature and it is lower than environmental temperature. It can be estimated using following equation:

$$T_7 = 0.0552 T_6^{1.5} \quad (10)$$

It is mentioned that in Eq. (10) the relative humidity was not considered.

By considering energy conservation the energy balance equations for each points of the receiver per length of the collector is obtained as follow:

$$\dot{Q}_{loss} = \dot{Q}_{conv,1-2} = \dot{Q}_{conv,3-4} + \dot{Q}_{rad,3-4} = \dot{Q}_{cond,4-5} = \dot{Q}_{conve,5-6} + \dot{Q}_{rad,3-4} \quad (11)$$

2.4.2. Thermal analysis of parabolic concentrator

The heat loss coefficient of the receiver considering the area of concentrator, radiation information of the system and optical properties of the reflector can be calculated as follow (Duffie and Beckman, 2013):

$$U_L = \frac{\dot{Q}_{loss}}{\pi D_{ro} L(T_3 - T_6)} \quad (12)$$

The collector useful heat gain per unit length of the reflector can be calculated using heat removal factor (F_R) of collector and heat loss coefficient:

$$\dot{Q}_u = F_R A_a [S - \frac{A_r}{A_a} U_L(T_i - T_6)] \quad (13)$$

The quantity of F_R can be calculated based on the efficiency factor and flow factor of the collector.

2.4.3. Thermal efficiency of parabolic tube solar collector

The energy flux of a thermal system Q obtained according to the inlet (T_1) and outlet (T_2) fluid temperature:

$$Q = A\alpha(T_1 - T_2) \quad (14)$$

The useful energy produced by PTSC can be estimated using the energy balance in the fluid with the following equation (Yashavant et al., 2011):

$$Q_u = \dot{m} c_p(T_o - T_i) \quad (15)$$

The available thermal energy which produced by solar radiation (direct beam solar irradiation) can be written as Eq. (16) (Sharafeldin and Grof, 2018; Liangdong et al., 2010):

$$Q_s = A_a G_b \quad (16)$$

Q_s is defined as useful energy, A_a is collector surface (m^2) and G_b is direct solar irradiation.

According to ASHRAE standard 2003, thermal efficiency of PTSC was obtained (Samimi-Akhijahani and Arabhosseini, 2018):

$$\eta = \frac{Q_u}{A_a I_o} = \frac{\dot{m} c_p(T_o - T_i)}{A_a I_o} \quad (17)$$

2.4.4. Analysis of thermal storage tank

The other part of a thermal storage system is a tank which the fluid or PCM stored the thermal energy during sunny days. The whole parts of the storage tank is covered and insulated by glass wool. Moreover to increase the storage capacity, the spiral PCM tube was located inside the storage system. An electrical switch valve located at the inlet section of the tank. During the test days by increasing the solar radiation intensity the fluid temperature increases and consequently PCM temperature increases as well which called charging process. At this

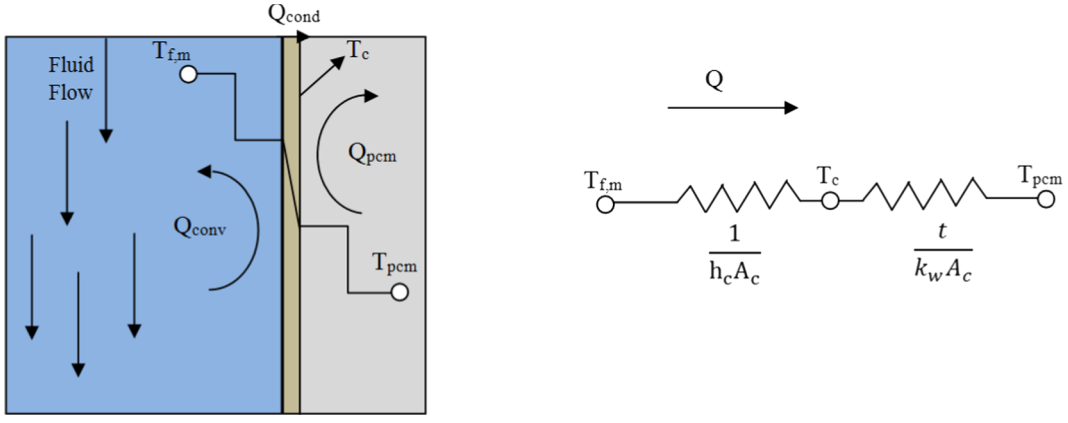

Fig. 4. The thermal circuit of wall (copper), PCM (as storage unit) and fluid flow.

condition the paraffin wax liquefied. After that by decreasing the fluid temperature due to lack of solar radiation PCM releases the stored thermal energy to the fluid flows through receiver and the phases of paraffin changes to the solid state. This process called discharging process. Fig. 4 depicted the electrically simulation of the energy flux and fluid flow around the copper tube containing paraffin wax (Xiaohong et al., 2011).

The rate of thermal energy for the storage tank considering fluid temperature flows through the system evaluated using as:

$$Q_f = \dot{m} c_p (T_{f,in} - T_{f,out}) \tag{18}$$

$T_{f,in}$, $T_{f,out}$ represents the value of inlet and outlet fluid temperature of container.

A part of thermal energy is transferred via tempered fluid to the tube wall via convection process (Q_{conv}) which can be calculated via Eq. (19):

$$Q_{conv} = h_c A_t (T_{f,m} - T_{w,m}) \tag{19}$$

Heat conducted to the PCM is expressed by (Holman, 2002):

$$Q_{cond} = k_w A_t \frac{(T_{w,m} - T_{pcm})}{t_w} \tag{20}$$

T_{pcm} represent PCM temperature.

There is two main process that occurred for PCM during heat transfer containing charging or discharging processes which can be calculated as (Goyal et al., 1998):

$$\begin{aligned} Q_{pcm} &= m_{pcm} c_s (T_{pcm} - T_{melt}) \quad T_{pcm} < T_{melt} \\ Q_{pcm} &= 0 \quad T_{pcm} = T_{melt} \\ Q_{pcm} &= m_{pcm} c_l (T_{pcm} - T_{melt}) \quad T_{pcm} > T_{melt} \end{aligned} \tag{21}$$

Some of the received thermal energy (E_{st}) stored in the fluid and the other stored in PCM which defined by Eq. (22) (Haller et al., 2009):

$$E_{st} = Q_f + Q_{pcm} \tag{22}$$

2.5. Drying efficiency

To evaluate the effect of using different fluids as working fluid used for heat transfer process on the drying of product, the drying efficiency must be considered. Drying efficiency describes by obtaining energies applied for heating the sample and extracting water over whole thermal, electrical and mechanical energies (Samimi-Akhijahani et al., 2017). For this purpose fresh Golden delicious apple (*Malus domestica*) purchased from a local market in Sanandaj, Kurdistan, Iran and placed in a refrigerator. The apples washed and then sliced into 7 mm thickness with a sharp knife. The moisture content of fresh apple samples was 83.9% ± 1% (w.b), measured by a standard oven dryer at 105 °C for 24 h. About 200 g of slice samples placed on clean trays and located inside the cabinet. The sample trays were weighed every 15 min at the beginning of drying hours and then by decreasing the moisture content it measured every 30 min. The samples were weighed by a precision digital balance with accuracy of 0.05 g and capacity of 1500 g. Moisture ratio of the samples calculated by Eq. (23) as follow (Motahayyer et al., 2018):

$$MR = \frac{M_t - M_e}{M_0 - M_e} \tag{23}$$

The variations of the drying rate of samples estimated based on the equilibrium moisture content and difference in moisture content at any time (Shanmugam and Natarajan, 2007):

$$DR = \frac{dM}{dt} = -k(M_t - M_e) \tag{24}$$

For calculating the drying efficiency (η_{dryer}) the consumed energy for drying of samples and the whole energy imported to the system was considered and it can be obtained by Eq. (25) (Vieira et al., 2007):

$$\eta_{dryer} = \frac{Q_{out,dryer}}{Q_{in,dryer} + E_{mec}} \tag{25}$$

The amount of thermal energy imported to the solar system $Q_{in,dryer}$ can be calculated by (Demir and Dincer, 2017):

$$Q_{in,dryer} = 10^{-6}[(\int_0^t \dot{m}(t) \times c_p (T_{in,coll} - T_{out,coll})dt) - \int_0^t \dot{m}(t) \times c_p (T_{in,s} - T_{out,s})dt)] \tag{26}$$

The amount of outlet energy from the solar system ($Q_{out,dryer}$) calculated by:

$$E_{o,dryer} = 10^{-3} \times W \times L_v \tag{27}$$

where W indicated the moisture extracted from the apple slices via drying process (kg) and L_v represents the moisture vaporization latent heat (kJ/kg) can be calculated using:

$$W = \frac{W_a(M_o - M_f)}{100 - M_f}, \; L_v = 2502.54 - 2.309 T_{ca} \tag{28}$$

Due to the higher moisture content of fruit the value of L_v is higher than grains.

A part of the energy used for drying process consumed for air circulation inside the dryer which supplied by a fan. The other part consumed by a pump considered in the system to circulate the working fluid in the storage system and heat exchanger represented by E_{mec} and it can be obtained by following equation considering operation time (s):

$$E_{mec} = 10^{-6} \times P_{fan \;\; or \;\; pump} \times t \tag{29}$$

2.6. Fundamentals of CFD theory

2.6.1. Solar absorber tube

The amount of thermal energy produced by solar radiation on each part can be estimated by Eq. (30):

$$Q_{rad} = A_e \sigma (T_c^4 - T_a^4) \tag{30}$$

where Q_{rad} is the thermal radiation power (W), A_e is radiation area (m^2), σ is Boltzmann constant 5.669 × 10^8 ($W/m^2 K^4$) and T_a and T_c represented the temperature (°C) of the ambient air and the tube (Holman, 2002).

The relation between the radiation and the absorption for the collector can be evaluated by Eq. (31):

$$\theta + \alpha + \tau = 1 \tag{31}$$

where θ is reflection coefficient, α is absorption coefficient and τ is diffusion coefficient. Generally most of the materials used to construct the thermal systems do not emit thermal and solar radiation, therefore its value was not considered in modeling process. The spectral coefficient as a required factor for modeling of solar systems can be calculated using Eq. (32) considering the flux of visible beams to the surface ($I_{visible}$) and the fluxes of infrared rays (I_{IR}):

Table 2
The characteristics of the working fluids and copper tube as the receiver of the collector.

Fluid type	Properties			
	Specific heat of Fluid (J/kg·K)	Thermal Conductivity of fluid (W/m·K)	Density (kg/m^3)	Viscosity (kg/m·s)
Water	4182	0.6	998.2	1.001×10^{-3}
Glycerin	2428	0.284	1261	0.799
Engine Oil	1980	0.96	917	0.96
NanoFluid	3756	1.103	1097	0.01
Copper	390	401	8920	–

Table 3
The properties of grid applied for the thermal storage system with metric size of meshes.

Property	Quantity or Quality
Meshing type	Fine
Minimum size	0.00005 m
Maximum size	0.00012 m
Number of Cells	Tube: 214564, Fluid: 432,761
Minimum angle	39.4°
Maximum angle	140°
Mesh metric	Skewness, 0.29
Pinch tolerance	0.0018
Standard deviation	0.1654

$$SF = \frac{I_{visible}}{I_{visible} + I_{IR}} \tag{32}$$

The radiant heat transfer equation can be obtained with consideration of the reflection and absorption in position r and direction s as Eq.33:

$$\frac{dI_{[\vec{r},\vec{s}]}}{ds} + (\alpha + \theta) I_{[\vec{r},\vec{s}]} = \alpha n^2 \frac{\sigma T^4}{\pi} + \frac{\theta}{4\pi} \int_0^{4\pi} I_{[\vec{r},\vec{s}]} \varphi_{[\vec{s},\vec{s}]} d\Omega' \tag{33}$$

Which n represents the light refractive index of, φ light fuzzy functions and'Ω the solid angle of the sun's motion.

The conjugation and displacement equations can be solved considering Eqs. (34) and (35). It is noted that gravitational acceleration was not considered in the modeling process.

$$\frac{\partial \rho}{\partial t} + \nabla . (\rho U) = 0 \tag{34}$$

$$\frac{\partial \rho U}{\partial t} + U . \nabla \rho U = -\nabla P \tag{35}$$

Reynolds number is one of the important factors significantly changes the simulation process of the systems such as solar collectors and it must be calculated for further progress. For all the conditions the Reynolds number was checked and the results showed that the proper model for fluid flow in the system is the turbulent models ($Re > 2400$) (Malekjani and Jafari, 2018). Thus fluid viscosity, turbulence and buoyancy was considered through the simulation to obtain the proper results of heat transfer, temperature contours and fluid distribution through the system. One of the most reliable and successful models which is widely used in agricultural and industrial fields is k - ε and verified by using experimental data (Babu and Gugulothu, 2015, Ambekar et al., 2016; Shih et al., 1995). Following two transport turbulent formula for CFD simulation model were introduced:

$$\frac{\partial}{\partial t}(\rho k) + \frac{\partial}{\partial x_i}(\rho k u_i) = \frac{\partial}{\partial x_j}\left[(\mu + \frac{\mu_t}{\sigma_k})\frac{\partial_k}{\partial x_j}\right] + G_k + G_b - \rho\varepsilon - Y_M - S_k \tag{36}$$

$$\frac{\partial}{\partial t}(\rho \varepsilon) + \frac{\partial}{\partial x_i}(\rho \varepsilon u_i) = \frac{\partial}{\partial x_j}\left[(\mu + \frac{\mu_t}{\sigma_\varepsilon})\frac{\partial_\varepsilon}{\partial x_j}\right] + C_{1\varepsilon}\frac{\varepsilon}{k}(G_k + C_{3\varepsilon}G_b) - C_{2\varepsilon}\rho\frac{\varepsilon^2}{k} + S_\varepsilon \tag{37}$$

Numerical procedure and modeling:

To analyze the fluid dynamics of the collector, ANSYS workbench 14.2 was considered. Moreover 3D model of the system with fully details was drawn by Solid works software V2016. Then, the 3D models saved in the separated files and then imported to fluent environment as subprogram of Ansys. Once the absorber tube has been modeled, material's types and boundary conditions applied to the model as well. According to the fluid condition (hydraulic diameter and fluid velocity) turbulence condition applied to solve the problem. The mesh size in this analysis is kept at normal condition. Four types of fluids are employed in the simulation part and with various properties as listed in Table 2. Physical properties of Al_2O_3 (as nanofluid used in working fluid) based on the physics of two used materials can be calculated as follow (Khanafer and Vafaei, 2011):

$$\rho_{nf} = (1 - \phi)\rho_f + \phi\rho_p \tag{38}$$

where ϕ, ρ_f and ρ_p are volumetric fraction of nanoprticle, density of base fluid and nanoparticle, respectively. For the nanoparticle it was about 3603 kg/m^3. Moreover the specific heat of nanofluid estimated considering heat equilibrium with fluid and added nanoparticles (Ghasemi and Ranjbar, 2015):

$$C_{p,nf} = \frac{(1 - \phi)(\rho C_p)_f + \phi(\rho C_p)_p}{\rho_{nf}}, \; C_{p,f} = 790.1 \;\; \text{J/kg·K} \tag{39}$$

Thermal conductivity of nanofluid (single phase) estimated using empirical following equation (Chon et al., 2005):

$$k_{nf} = k_f(1 + 64.7T^4\left(\frac{k_p}{k_f}\right)^{0.747}\left(\frac{d_f}{d_p}\right)^{0.369} Pr_f^{0.995} Re_f^{1.232} \tag{40}$$

where k_{nf}, k_f, d_f and $d_p$are thermal conductivity of nanofluid and base fluid, molecular diameter of base fluid and nanoparticls. *Pr* and *Re* are Prantdel and Reynolds numbers of base fluid. The nanofluid properties are embedded within the CFD simulation process which defined by a

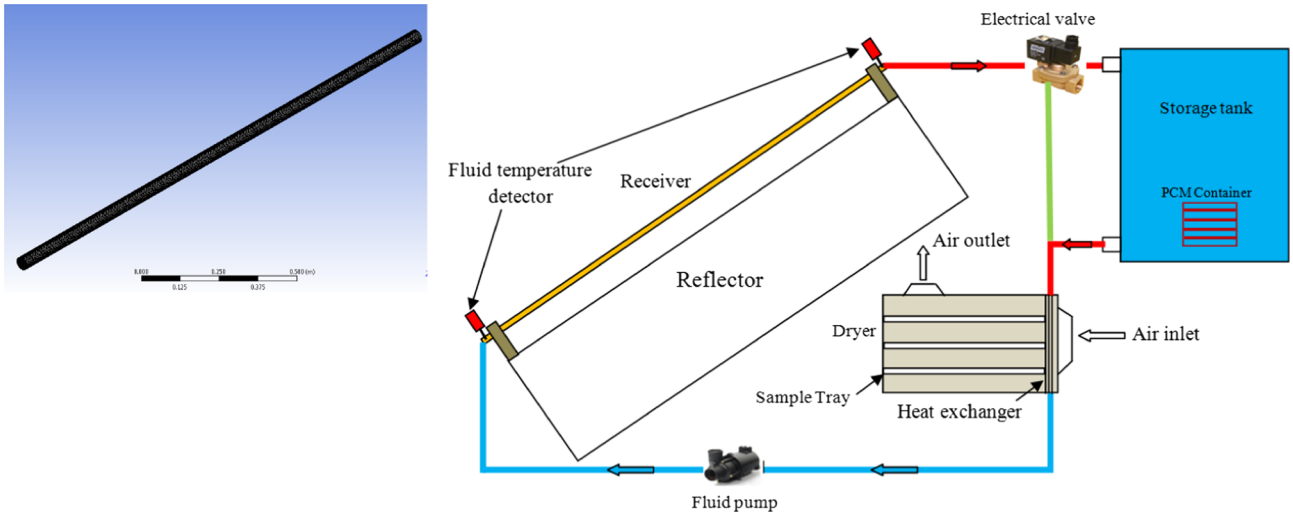

Fig. 5. The meshing schematic and the points considered for controlling the temperature variations of the receiver tube.

Table 4
The properties of grid applied for thermal storage tank with size of meshes.

Parameter	Quantity and Quality
Mesh type	Fine
Minimum size	0.00005 m
Maximum size	0.00012 m
Number of Cells	Tube: 113544, PCM: 496875, Fluid: 1,734,524
Min angle	39.4°
Max angle	140°
Mesh metric	Skewness, 0.41
Pinch tolerance	0.0018
Standard deviation	0.1654

user-defined function.

For modeling the receiver tube a 3D model with steady state turbulent condition with k-ε RNG was considered. Moreover standard wall functions with the SIMPLEC solution algorithm applied to simulate heat transfer process in the receiver tube. For the tube with non-equilibrium (no homogenous) wall functions the k-ε RNG resulted an acceptable prediction of the thermal process (Tzirtzilakis and Kafoussias, 2010). For momentum and energy equations applied for the simulation process, the second order upwind differencing code was considered. The limit ranges for convergence criteria for the scaled residuals was set to 10^{-4} for momentum and mass equations, and 10^{-5} for the energy equation.

The mesh quality for the model was checked using skewness index by statistical parameters. Typically, the value of the mesh skewness varies between 0 and 1 which the mesh near to zero is the best and the mesh near to 1 is the worst (Brandl et al., 2015; Karmare and Tikekar, 2010). The fine mesh was considered for receiver tube and determination of meshing process illustrated the obtained skewness for the system was about 0.29 which is acceptable. Thus fine mesh can be used for any progress in CFD simulation. The details listed in Table 3. The data obtained from the software are compared with experimental data under different conditions of fluid flow rate in collector and the appropriate mesh is selected. The time taken to solve the problem and the analysis using very fine, fine and course meshes, was about 4 h and 30 min, 1 h and 25 min and 45 min, respectively. Considering that the difference between the data obtained from very fine and fine mesh was not significant, so the fine grid was used to continue the analysis. For validation of the model, outlet temperature of the tube was considered and the results showed that the model with the maximum error of 3.2% has a good agreement with the theoretical outputs. The grid independency test was used to test the accuracy of the selected grid and it showed that the selected mesh was the most suitable mesh for this simulation process.

Boundary conditions: The following boundary conditions were investigated for simulation the receiver tube:

Inlet: the fluid flow for all the experiments was uniform velocity with uniform temperature. Wall: the top and bottom half periphery of the tube are subjected to the radiation. The concentration ratio of the collector is assumed about 25 and only less than half of the pipe receives the solar radiation which reflected by parabolic concentrator. A uniform heat flux was considered for the walls. Outlet: the pressure gradient at the outlet section is assumed equal to zero. The fluid temperature at the inlet and outlet section was recorded to detect the thermal gradient of working fluids. Thus two K-type calibrated thermocouples connected to a data logger used to record and store the temperature of defined points every 30 min. The position of thermocouples depicted in Fig. 5.

2.6.2. Thermal storage tank

To model and simulate the cylindrical storage tank considering the PCM, mass, momentum and energy conservation equations in coupled condition were considered. Eqs. (41)–(43) represents the continuity, Navier–Stokes and energy equations (Tay et al., 2012a; Singh and Singh, 2018).

Due to the properties of the fluid flows inside the system the incompressible, laminar and unsteady conditions at three dimensional was considered. Moreover the viscous loss for the fluid was negligible.

Continuity equation:

$$\nabla . \vec{V} = 0 \tag{41}$$

Momentum equation in all direction:

$$\frac{\partial \vec{V}}{\partial t} + \vec{V} . \nabla \vec{V} = \frac{1}{\rho}(-\nabla P + \mu \nabla^2 \vec{V} + \rho \vec{\beta g} (T - T_{ref}) + \vec{S} \tag{42}$$

Due to the properties of materials, phase changing process affects on convection process, thus momentum source term identified by $\vec{S}$ considered in Eq. (42). Moreover the dynamic viscosity of PCM identified by μ as a function of temperature:

$$\mu = 0.82 e^{0.0155 . T_{pcm}} \qquad 325 < T_{pcm} < 356 \tag{43}$$

The calculations of thermal energy:

The thermal energy equation of storage system is considered by:

$$\frac{\partial h}{\partial t} + \frac{\partial H}{\partial t} + \nabla \cdot (\vec{V} h) = \nabla \cdot (\frac{k}{\rho c_p} \nabla h) \tag{44}$$

Where h presented the enthalpy of all material used in storage system considering the reference enthalpy (h_{ref}) at reference temperature (T_{ref}) and latent heat content (H) and it expressed using Eq. (45) (Lacroix, 1993):

$$h = h_{ref} + \int_{T_{ref}}^{T} c_p dT, \; H = h + \Delta H \tag{45}$$

The reference enthalpy varies between zero (for PCM at solidus condition) to one (for PCM at liquid condition). Due to the phase changing during the thermal process the liquid fraction (ξ) must be considered based on PCM temperature:

$$\xi = \begin{cases} 0 & if \quad T_{pcm} < T_s \\ 1 & if \quad T_{pcm} > T_L \\ \frac{T - T_s}{T_L - T_s} & if \quad T_s < T_{pcm} < T_L \end{cases} \tag{46}$$

Knowing the liquid fraction of PCM the value of momentum $\vec{S}$ estimated considering mushy zone constant (A_{mush}) as:

$$\vec{S} = \frac{(1 - \xi)^2}{\xi^3} A_{mush} \vec{V} \tag{47}$$

Generally, A_{mush} (as constant value through the modeling to explain the kinetic process) due to the volume fraction and porosity inside the solid phase changes between 10^4 and 10^7 and for this project it is assumed to be about 10^5.

Boundary conditions:

The problem for the system was considered steady state and the

Table 5
The characters of paraffin wax used in the study (made by Iran Paraffin CO.)

Character	Thermal Conductivity (W/m K)	Specific heat (kJ/kg K)	Oil content	Density (kg/m^3)	Melting point (°C)	Kinematic viscosity at 100°C (Cst)	Latent Heat (J/kg)
Quality Or Quantity	0.19	2.17	0.5%	779	54	6.13	169

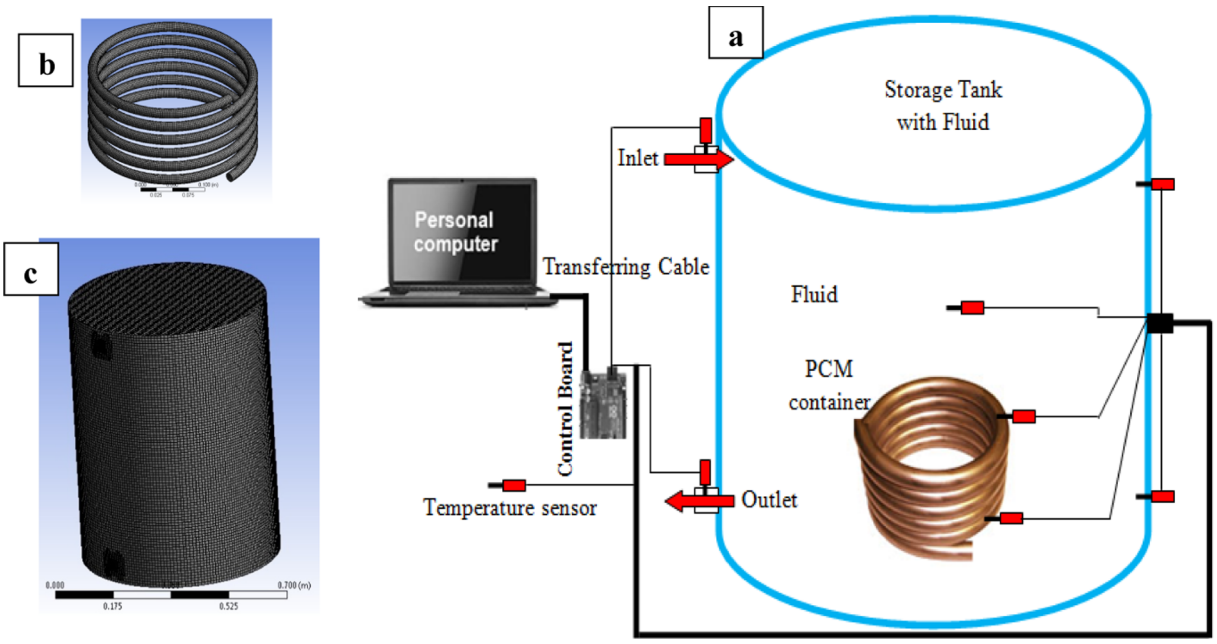

Fig. 6. (a) The points considered for controlling the temperature variations of the storage tank containing PCM and fluid, (b) 3D view of applied mesh for PCM and (c) storage tank.

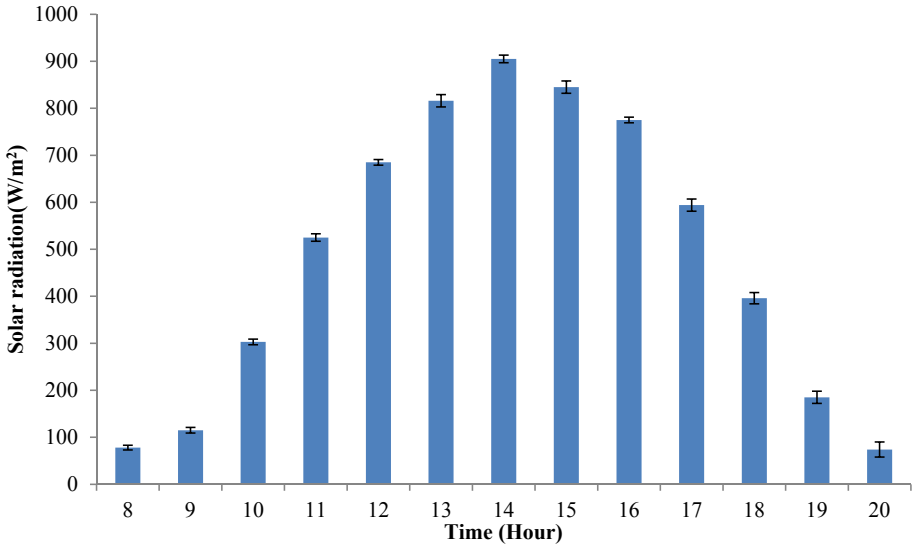

Fig. 7. Fluctuations of solar radiation for different fluids along the test days.

environmental temperature was considered as the initial condition. Due to the little difference between the conditions of the fluid flows in the storage system the flow pattern was the same. Based on the Reynolds number (lower than 2000) laminar pattern introduced the best pattern for the system. There are two states for the storage system including charging and discharging which PCM changes the phase during the mentioned processes. The velocity with normal to the boundary condition at the inlet fluid section was entered according the average amount of the mass flow rate. The walls of storage tank and PCM container was considered as stationary condition. For the storage tank, insulation walls was applied as well. For each section different heat flux was imported.

Frictionless with smooth condition was considered for the entire surface which fluid flows through the tank and PCM. During the steps of CFD analysis it was assumed that the ambient temperature is constant and the outside pressure has not any effect on the analysis. 3D mesh was applied to the storage system and the quality of applied mesh was checked statistically using skewness index and it obtained about 0.41 for this system which was suitable for CFD simulation. To ensure the proper use of mesh, grid independency test was applied and the results considering the consumed time indicated that fine mesh was a proper mesh for simulation of the storage tank. The quality of the grid size and meshing parameters are presented in Table 4.

Paraffin is a derivative of petroleum with non-renewable property that used in both solid and liquid form. In this study the solid form with low oil content (lower than 0.5%) was considered. Paraffin wax used in this study was purchased from “Iran paraffin Company”, with at least two year life time without any corrosion and change of properties during phase changing process. The chemical, thermal and physical characteristics of paraffin as PCM are presented in Table 5.

Since the pressure-based model reported as a proper model to express melting and solidification processes of PCM, thus it used to any

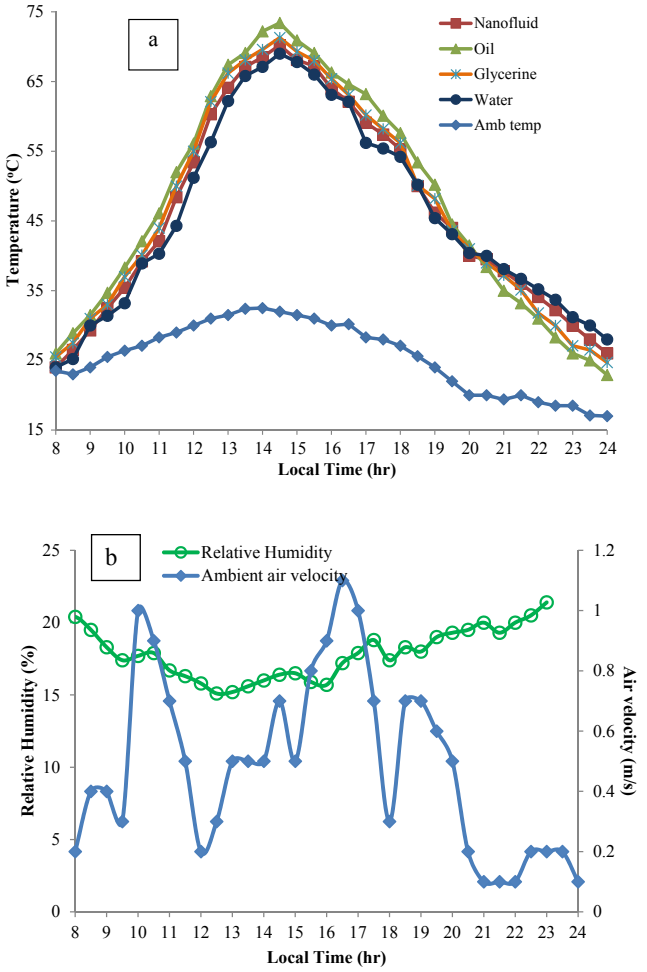

Fig. 8. Variations of (a) temperature inside the cabinet with four types of working fluids, (b) mean ambient air velocity and relative humidity along the test days.

progress in simulation (Lacroix, 1993; Al-abidi et al., 2013). For convergence criteria 10^{-5} was applied as limit range of energy equation and for continuity and momentum equations it considered about 10^{-4}.

About seven K-type thermocouples were located in the container (storage tank) to record temperature changes 30 min during charging and discharging process. The points were showed in Fig. 6.

For CFD simulation of receiver tube and storage system Ansys – Fluent was selected which is the proper software increasingly used for thermal analysis of the systems with fluid flow. 3D model of each system designed in ANSYS workbench V 15.0.0. Then meshing process was applied to 3D modeling (ICEM) using available grids (Fig. 6b,c). By meshing the model now it is ready for applying the identified the boundary conditions including fluid and solid regions. By applying the boundary conditions the problem solved considering the defined solution methods, and finally the results extracted in the form of graphs with counters and or streamlines.

Typically based on reasonable amount of the accuracy number of repeating of the process was determined. In the other words, the number of iteration is defined by considering the desire targets for velocity, pressure and temperatures which in this study it was set on 1500. Therefore the convergence value (criteria for the solution errors) for the present project was considered about 10^{-4} and when it fell below 10^{-4} solving process of the model stopped. To prove the accuracy of CFD model the relative error between predicted (Pre) and experimental (Exp) data was used (Eq. (48)) (Hung et al., 2017; Gunjo et al., 2017, Arabhosseini et al., 2019):

$$Er(\%) = \frac{|D_{pre} - D_{exp}|}{D_{pre}} \times 100 \tag{48}$$

2.7. Evaluation the quality of dried samples

In most systems which used new technologies for increasing the performance of the system the quality of obtained product decreases and the price of the dried product reduces. Therefore it will not be marketable to sell dried product and the method with new technology was not recommended for any drying process. Three main parameters were considered for quality consideration including color, shrinkage and rehydration ratio. Each day after drying process, the dried slices put in a tray at room temperature (about 20–25 °C) for about an hour and the quality of the sample were taken in six replications.

First of all color evaluation of the samples was considered. For this purpose a 400 × 400 × 600 mm^3 laminated wooden cube box with a digital high resolution (about 10 MP) camera (Canon, type A3200 IS, Made in Japan), two 23 Watt fluorescent lamp for homogeneous lighting and black background (to minimize the impact of light or shade noises) were provided. The taken images saved in graphic format (JPEG), analyzed using “Image Processing subprogram of Matlab program” and the intensity of red (R), green (G) and blue (B) was evaluated in the range of 0 to 255. The color changes defined by considering the variations of the slices occurred during drying process:

$$\Delta E_{RGB} = \sqrt{(R - R_0)^2 + (G - G_0)^2 + (B - B_0)^2} \tag{49}$$

Shrinkage of dried samples is the other parameter used for evaluation the quality. During the drying of apple slices due to diffusion coefficient the volume of the product changes. The variation of shrinkage is calculated according to the fresh condition of the sample. The complete description of shrinkage measurement with details is mentioned in Samimi-Akhijahani and Arabhosseini (2018). Shrinkage of dried slices can be expressed using (Moreira et al., 2000):

$$S_b = 1 - \frac{V}{V_0} \tag{50}$$

The third quality assessment of dried samples is the rehydration ratio and it can be calculated by defining the amount of water absorbs by dried product. For this purpose about 25–30 g of samples soak in distilled water at boiling temperature. The samples taken out of the water container after 5 min, dried with a clean tissue put on the digital balance and weighed again (Sacilik and Elicin, 2006; Doymaz, 2010). The rehydration ratio (RR) was obtained by Eq. (51) considering rehydrated (W_r) and initial (W_d) weights (Samimi-Akhijahani and Arabhosseini, 2018):

$$RR = (\frac{W_r}{W_d}) \tag{51}$$

3. Results and discussions

Fig. 7 demonstrates the fluctuations of solar radiation versus local time during the test days. By the time the solar radiation intensity increased and at around 14:00 the maximum value recorded. The highest radiation intensity occurred at around 13:00–15:00. It increases and decrease along the test days and changes from 74 to 905 W/m^2. Fig. 7 also shows that the fluctuations of the solar radiation are not significant during the experimental days.

The variations of the fluid temperature in the drying cabinet, ambient relative humidity and temperature and air speed during the experimental days are shown in Fig. 8. By increasing the radiation intensity, more thermal energy absorbed by receiver tube (located at the focal line of the collector, covered by glass and painted in black). The fluid flows through the tube and the average fluid temperature increases as well. At the end of the day (18:00–20:00) the solar radiation

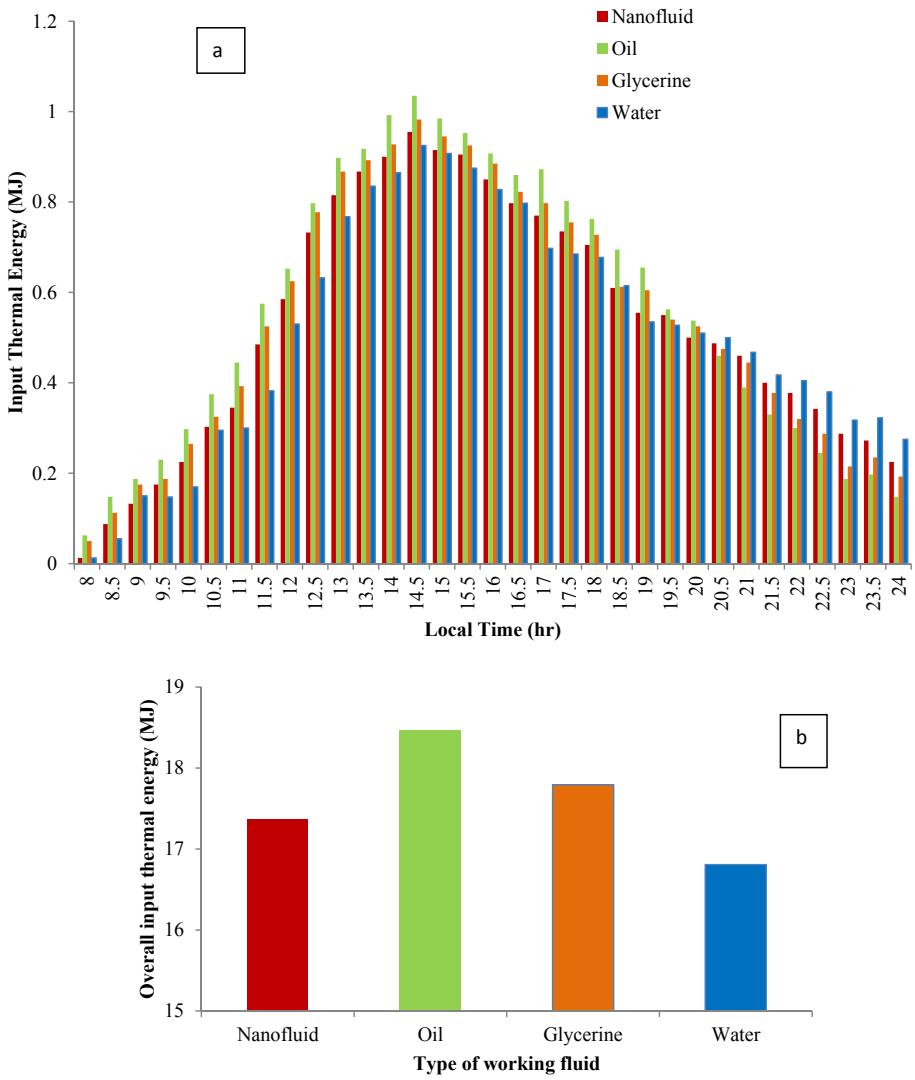

Fig. 9. The variations of (a) thermal energy entered to the dryer via local time, (b) overall (total) thermal energy inserted to the dryer with different working fluids.

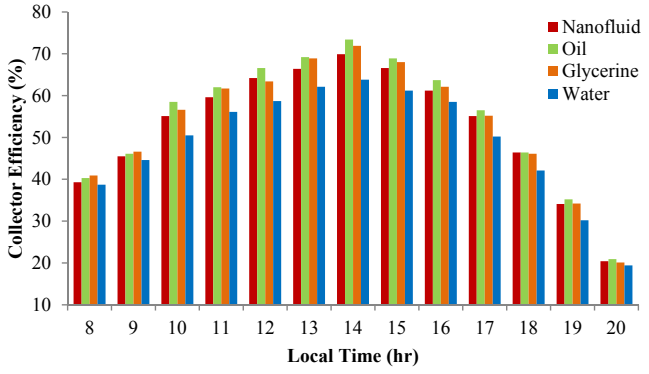

Fig. 10. Hourly thermal efficiency of PTSC with different working fluid versus local time.

decreased and consequently the increasing rate decreased as well. Due to have the difference of the heat capacity, the temperature values of fluids in the tank was different. The higher temperature for water, nanofluid, glycerine and engine oil were about 69 °C, 70.2 °C, 71.3 °C and 73.4 °C, respectively. During the test days the ambient air temperature was varied from 17 °C to 32.5 °C and the relative humidity changes from 15.1 to 22.6% during the drying days. Moreover, the air speed varied from 0.1 m/s to 1.1 m/s.

Fig. 9(a) indicated thermal energy entered to the drying cabinet with four types of working fluids inside the solar drying system. For all condition the phase change materials were located inside the storage tank. The figure shows that for all types of working fluids the input thermal energy varies with variation of radiation intensity and it increases and decreases by increasing and decreasing radiation. Due to the thermal properties of the fluids (heat capacity and thermal conductivity) the rate of increasing and decreasing thermal energy was different. For water (as working fluid) due to higher heat capacity the time for increasing temperature of the fluid is higher than other fluids (especially at 8:00–14:00). In the other words it takes more time to increases the temperature of water. After the sunset due to higher stored thermal energy in water, the time for discharging process is higher. Overall (total) input thermal energy to the cabinet using different working fluids is illustrated in Fig. 9b. The maximum (18.46 MJ) and minimum values (16.80 MJ) was related to the dryer with working fluids of oil and water, respectively. The air mass flow rates for drying system for all experiments was about 0.025 kg/s. Using nanofluid improved the amount of input energy and increase it up to 3.27% compared to the water system. Moreover, the thermal energy for oil and glycerine was higher and it was about 10.12% and 6.02%, respectively. The investigation on the thermal energy produced by PTSC are reported the same results (Kumaresan et al., 2012; Zhao et al., 2009, Motevali,

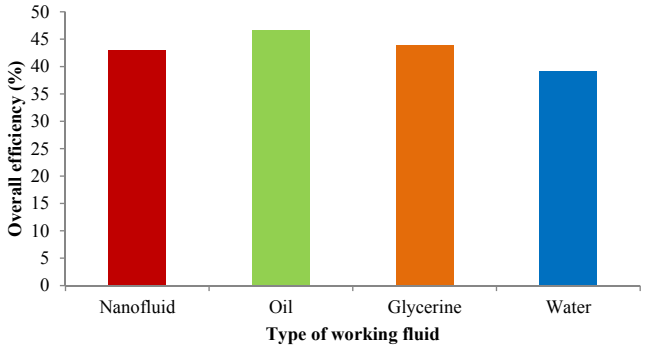

Fig. 11. The obtained overall drying efficiency of the system with different working fluids.

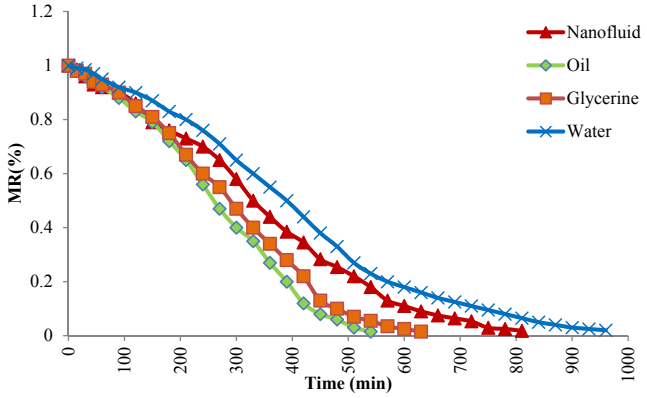

Fig. 12. Variation of MR against time (min) consumed to dry apple samples with different working fluids.

2013; Khosravi et al., 2019; Abbood and Mohammed, 2019; Mwesigye et al., 2015).

One of the main parameters which clarified the performance of a solar system is thermal efficiency. Fig. 10 depicted the variations of thermal energy efficiency of the parabolic tube solar collector. It increases with increasing with the time from 8:00 to 14:00 and then decrease. In the other words in the morning and in the evening the solar radiation is low and the cosine loss is high (Wang et al., 2016). Thus the collector efficiency in the mentioned times is lower. The accurate solar tracking system could improve the cosine loss and consequently thermal efficiency (Kalogirou, 2009). Moreover the rate of increasing thermal efficiency of the collector from 10:00 to 16:00 is lower. The value of collector efficiency for nanofluid, oil and glycerin is higher than water as working fluid about 5.83%, 9.27% and 7.67%. The maximum efficiency of the collector with different working fluids is about 69.9%, 73.4%, 71.9% and 63.8% for nanofluid, oil, glycerin and water, respectively. Due to higher thermal conductivity, more solar radiation absorbs by nanofluid and the thermal efficiency increases (Khosravi et al., 2019).

Fig. 11 shows overall energy efficiency of solar dryer. It was containing the electrical, mechanical and thermal energies which consumed to dry the samples. The overall thermal efficiency varies by changing the type of the working fluid. By increasing the drying time, the electrical and mechanical energy used for drying process increased. One of the important parts of the efficiency is reducing the energy consumed by electromotor, hydraulic pump and fan. When the drying time reduces the power used by the mentioned elements reduces as well. This leads to improve the overall efficiency. In the other words the value of specific moisture extraction rate (SMER) from slices increases. Thus, the overall efficiency for the systems with water and nanofluid are lower than engine oil and glycerin. The highest (46.65%) and lowest (39.11 MJ) values was related to oil and water as working fluids, respectively. The using submerged nanoparticles in water as base fluid, increases the heat transfer coefficient. It also implied that using Al_2O_3 improved local heat transfer coefficient of the collector tube and this improved the output temperature of the collector. It can be seen that using different types of the fluid (glycerin, engine oil and nanofluid) improved the overall efficiency of the collector. The other factor affects on the overall efficiency of the drying system is the drying air with higher temperature which exhausted from the dryer. Using the recycling system with controlling valves saves most of the thermal energy and it can be consumed for drying of the products. Similar results were reported by other researches that used solar system to supply thermal energy in dryers (Motevali, 2013; Ruvinda et al., 2011; Yadav et al., 2013).

The variation of moisture ratio (MR) against the drying time for the solar dryer with different working fluids graphically showed in Fig. 12. For all conditions the air flow rate of drying process was about 0.025 kg/s. The drying rate of apple slices (placed on the trays inside the cabinet) at the beginning of the drying process was lower because of the less solar radiation. Then with increasing radiation intensity more thermal energy transmitted to the fluid and consequently the amount of

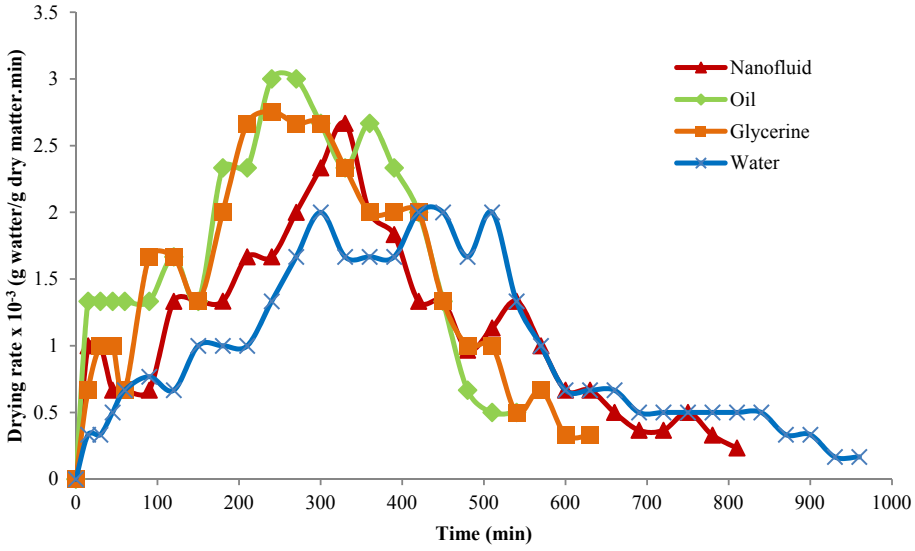

Fig. 13. Variation of MR against the time (min) consumed for drying of slices with different working fluids (Nanofluid, Oil, Glycerine, Water).

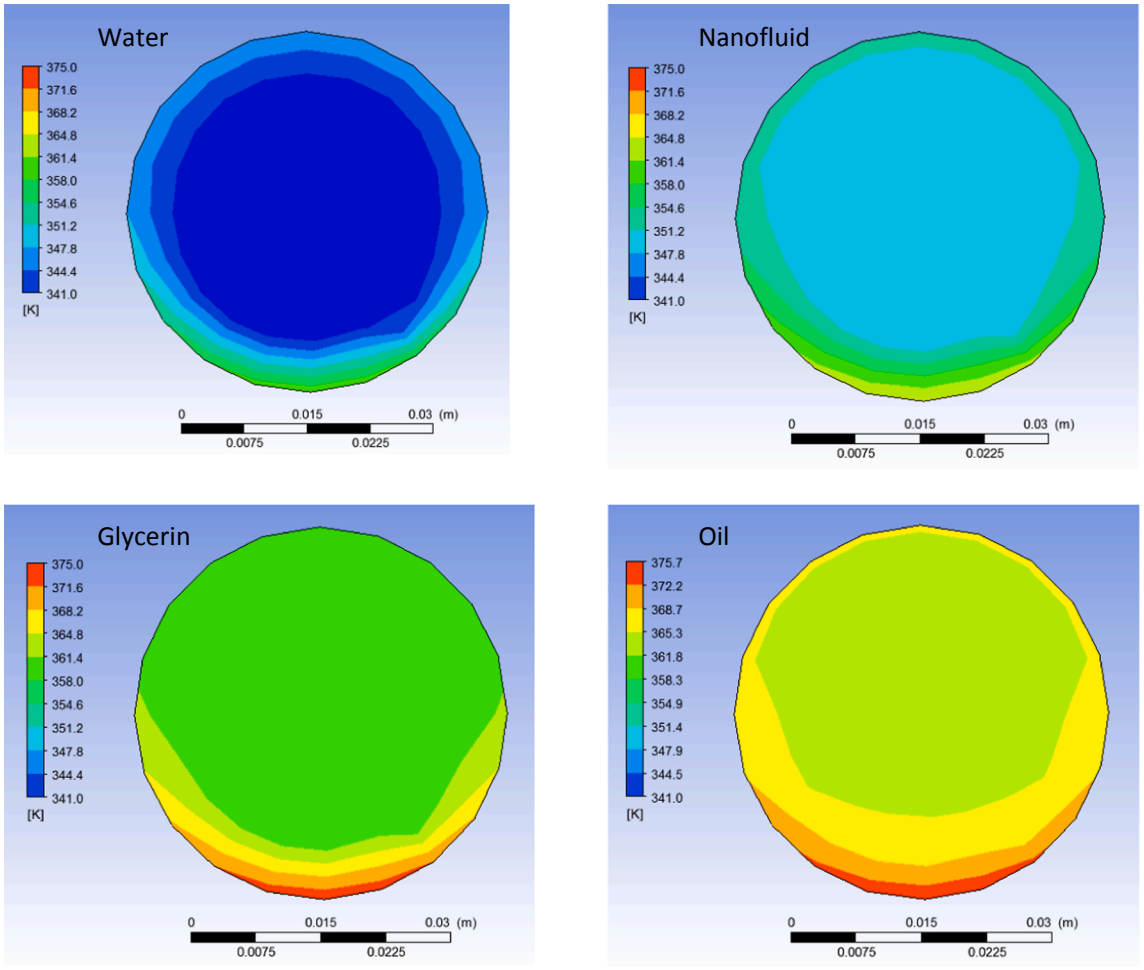

Fig. 14. Temperature Counters of receiver tube for different types of working fluid.

inlet energy to drying cabinet increases and the drying rate improved. The slop of the moisture ratio at the first times of drying is higher. At this condition the moisture in the texture of the apple slices (called free water) evaporated with lower thermal energy and the capillary effects of the tubes in the tissue helps to conduct the thermal energy to the bottom layers of samples. Then by decreasing the radiation intensity (after 15:00) free water declined, the thermal energy demand for evaporation of the slices increases and the time consumed for drying process increased. The time for drying of fresh apple samples dried by present dryer was varied from 540 to 960 min. Fig. 12, also showed the time consumed for drying process using nanofluid, oil, glycerin and water was 810, 540, 630 and 960 min. In the other words using different working fluids decreased the drying time about 15.62%, 43.75% and 30.32% relate to water.

Due to the higher moisture content of biological products during dehydration process of samples happens in two main levels. At the first level due to more moisture content on the surface, the water extraction from the product is higher. A part of thermal energy inserted to the cabinet consumed to evaporate water from outer surface of the slices and the other part moved to the internal texture to heat the product. In the other words the capillary force between water molecules enhances internal mass transfer of the slices (Arabhosseini et al., 2019). In the second level of drying process via hot air, there is no capillary force and mass transferring process takes place on the surface of the slices (Doymaz, 2010; Aghbashlo et al., 2008). This level is known as the falling rate. The mentioned report is consistent with the other results obtained from drying apple slices (Doymaz, 2010; Sacilik and Elicin, 2006).

At the first stage (Fig. 13) due to the high moisture content, water movement from the slices is higher and main part of drying of the slices happens at this stage known as falling rate period. At this condition, internal mass transfer occurs with liquid diffusion, vapor diffusion and inner capillary forces inside the samples and water moves to slice surface. Thus the thermal energy leads to evaporate it. Because of the capillary property of the slices and also the porosity structure which affects on drying rate, the water removes from the slices with lower thermal energy (Aghbashlo et al., 2008). At the second stage the free moisture removes from the fruit surface thus the shrinkage of the slices happens. At this condition pores and free spaces decreased, the rate of water removal diminished and heat transfer reduced significantly. Due to the lower drying time the shrinkage process occurred at the final stage especially when the power is higher. The effective diffusion coefficients (D_{eff}) can be obtained considering this fact that the slop of the variation of falling rate is almost constant. Moreover, Fig. 13 illustrated that with changing the working fluid, the drying rate changed consequently. The value of drying rate for the system with oil as working fluid because of the more thermal energy which stored in storage tank is higher. More heat was generated inside the slice and this leads to create high vapor pressure difference between the outer surface and the centre of samples. Such an influence of drying condition on the drying rate of samples resulted by previous studies (Evin, 2011; Darvishi et al., 2016; Eltawil et al., 2018, Samimi-Akhijahani et al., 2016). Drying rate increased with increasing solar radiation and the higher value occurred at around 13:00–15:00.

Fig. 14 displayed the results of CFD simulation and the contours of temperature at the outlet section of receiver tube for different types of working fluids at 12:00 o'clock (at noon time). The contours showed that in the bottom section of the receiver tube the temperature is higher

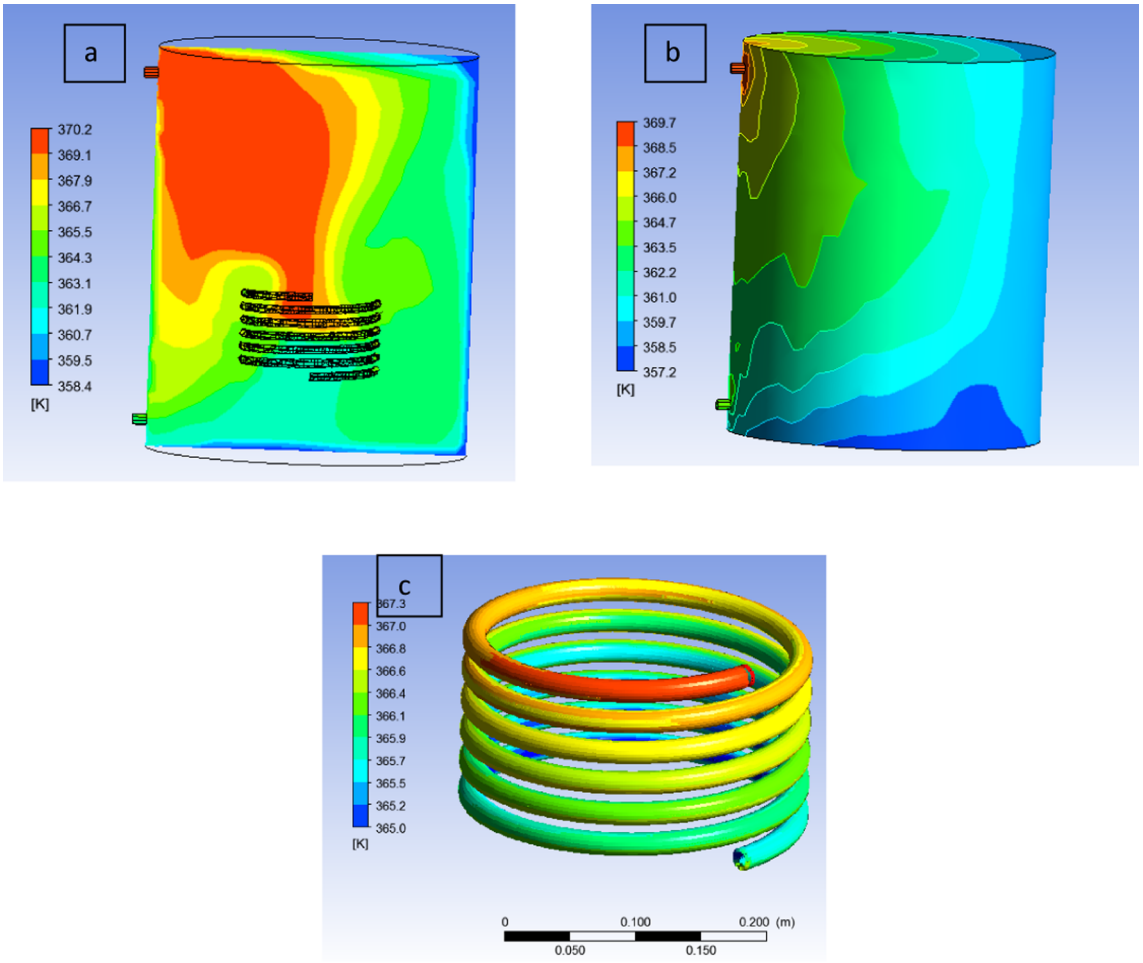

Fig. 15. Temperature contours for the thermal storage tank containing phase change materials at 12:00 with air flow rate 0.025 kg (charging process).

due to the higher radiation which reflected from the parabolic sheet. The core of the receiver tube has lower temperature. Because heat transfer takes more time to get the core of the fluid flow via convection process, especially when heat transfer coefficient is lower. The maximum and minimum outlet temperature for working fluid was related to engine oil and water (due to lower and higher specific heat capacity), respectively. It was varies from 342.3 K to 361.7 K for water and 347.9 to 363.2 for nanofluid and it indicated that by adding about 4% of volume fraction of Al_2O_3 nanopraticles the fluid temperature increased at least 5.23%. Moreover, because of the contact of nano-particle solution with receiver wall, more thermal energies absorbed and this decreases thermal loss (Khosravi et al., 2019).

The variation of temperature contours for thermal storage tank containing PCM and oil as working fluid simulated by CFD and the result presented in Fig. 15. The figure displayed the charging process of the storage tank at 12:00 when the air mass flow rate is about 0.025 kg/s. The result of CFD analysis and the variation of temperature contours presented that the higher temperature is related to the fluid located in the upper part of tank. The fluid flows through the tank and spiral tube, charges PCM via convective and conduction process (Fig. 15a). Moreover the figure illustrated that a part of the stored thermal energy loosed by the walls of the tank (Fig. 15b). However, this value is negligible due to the insulation around the tank. By moving the fluid from the inlet section to the outlet section and through the spiral tube, some of thermal energy stored in PCM and consequently increases paraffin temperature as shown Fig. 15c. The value of temperature difference at the top section and bottom section is around 2.3 °C.

When the solar radiation intensity reduces the reflection of the solar radiation decreases and the collector tube receives lower thermal energy. Consequently the fluid temperature at the outlet section of tube decreased. At this condition the electric valve cuts the fluid flow through PTSC and it flows to the dryer, directly. Fig. 16 presented the variations of temperature counters during discharging condition at 24:00 (when the ambient temperature is the lowest). The fluid temperature inside the tank is higher in comparison with the ambient temperature. Therefore the amount of energy stored in paraffin was released some of its energy to the fluid (Fig. 16a). Moreover temperature of the contours near the PCM is higher related to the other sections (almost 5–7 °C). Released thermal energy increases the temperature of the fluid inside the tank and then flows to the heat exchanger located at inlet section of drying cabinet. This leads to increase the input air temperature considered to dry apple slices especially at night times when there is no solar radiation. Fig. 16c displays the temperature variations of PCM counters at discharging condition for 0.025 kg/s as air flow rate. Same results were reported by the other researches which used PCM for improving thermal efficiency of the thermal systems (Kumaresan et al., 2012;Tay et al., 2012a).

To ensure the compability of the data obtained by experimental and CFD method the outlet temperature of receiver tube and storage tank with PCM were compared and listed in Tables 6 and 7, respectively. The presented data is related to different working fluids. According to the tables the fluid temperature at the beginning stages of the test increases and then reduces by fluctuation of the solar radiation along the test day. The results obtained from the research are in a good agreement with the results reported by other works studies on CFD simulation of thermal systems (Iranmanesh et al., 2020; Motahayyer et al., 2018; Jaramillo

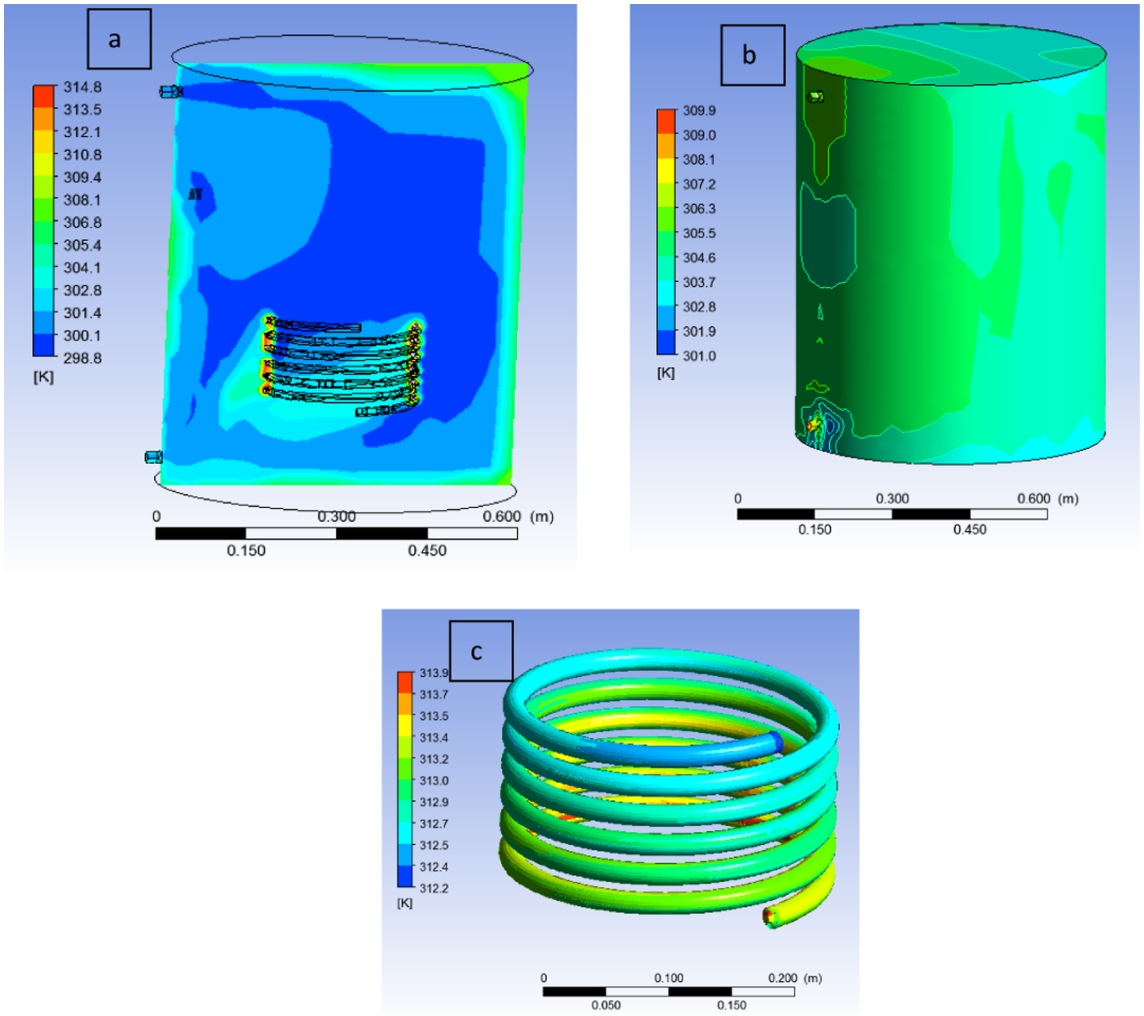

Fig. 16. Temperature contours for the fluid, walls of tank and PCM at 24:00 with 0.025 kg/s for air mass flow rate (discharging process).

Table 6
The comparison between the experimental and predicted temperature values (°C) for the receiver tube at different working fluids.

Experimental					Predicted by CFD			
Time	Nanofluid	Oil	Glycerine	Water	Nanofluid	Oil	Glycerine	Water
8	26.5	28.4	27.2	25.1	26.825	32	28	24
8.5	28	30.2	28.3	26.9	30.1	32	25.5	25
9	31.4	34.3	32.2	31	32.97	36	30	30
9.5	35.2	40.1	35.5	32.4	32	40.3	34.5	34.02
10	38.2	42.7	40.8	35.4	38.11	42.3	43	37.17
10.5	46.3	51.3	47.8	44.7	50.615	56	53	44.3
11	49.5	52.3	50.6	46.6	50	56.2	54.2	48.93
11.5	57.3	61.7	58.3	55.7	55	62.6	61.215	55.7
12	61.6	63.9	62	58.5	66	70.3	67.4	61.425
12.5	65.1	70.4	67.2	63.5	70	75.8	72.3	68.5
13	72.1	74.8	72.9	69.8	77.705	80.5	74	70
13.5	73.3	75.2	73.4	70.2	78.915	85	79.2	73.71
14	75.1	80.4	76.8	73.5	78.855	84.42	79.2	72.4
14.5	74.2	80	76.9	73	80.2	87.3	83.2	76.65
15	73.6	78.3	75.2	72.5	73	78.3	74.2	73.2
15.5	73.2	75.2	73	72	74	78.96	76.65	75.6
16	72.3	74.6	72	71.5	73	72	74	75.075
16.5	69.8	71.4	69.8	67.8	75	72.3	73.29	67.8
17	64.9	69.3	66.6	63.4	68.145	70.2	69.93	64.7
17.5	62.8	65.2	63.5	60	62	68.46	66.675	60
18	58.3	62.5	60	58.2	59.6	62.3	66	57.5
18.5	55.2	60.1	56.2	56.1	55.1	61.3	59.01	54
19	50.2	57.1	53.4	51.2	54.1	58.2	56.07	55.4
19.5	45.4	52.3	47	45.9	45.1	50	43	42
20	41.2	43	42	43	44.2	42	45	46

Table 7
The comparison between the experimental and predicted temperature values (°C) for the storage tank tube at different working fluids.

Experimental					Predicted by CFD			
Time	Nanofluid	Oil	Glycerine	Water	Nanofluid	Oil	Glycerine	Water
8	25.1	27.3	27	24.5	25.425	30.9	27.8	23.4
8.5	27.3	29.3	28	27.2	29.4	31.1	25.2	25.3
9	30.3	33.5	31.4	32	31.87	35.2	29.2	31
9.5	33.5	38.5	35	33.4	30.3	38.7	34	35.02
10	37.4	40.3	38.5	34.9	37.31	39.9	40.7	36.67
10.5	41.2	46.5	43.2	40.9	45.515	51.2	48.4	40.5
11	44.1	49.2	47.2	42.5	44.6	53.1	50.8	44.83
11.5	55.4	56.4	55.3	49.3	53.1	57.3	58.215	49.3
12	57.4	60.6	59.2	55.2	61.8	67	64.6	58.125
12.5	63.3	64.9	65.2	60.2	68.2	70.3	70.3	65.2
13	68.1	69.4	69.1	67.2	73.705	77.9	76	67.4
13.5	69.1	72.4	70.1	68.8	74.715	79.8	75.9	72.31
14	72.5	76.3	74.2	71.1	76.255	76.3	76.6	70
14.5	72.2	77.2	73.3	71	78.2	78	75.2	74.65
15	70.1	73.1	72.1	69.8	69.5	73.1	71.1	70.5
15.5	70.2	71.9	70.5	70	71	75.66	74.15	73.6
16	69.3	71.3	70	67.1	70	68.7	72	70.675
16.5	65.1	68.2	66.3	65.1	70.3	69.1	69.79	65.1
17	61.1	66.9	63.4	59.7	64.345	67.8	66.73	61
17.5	59	62.1	60.2	58.3	58.2	65.36	63.375	58.3
18	57.3	59.6	58.2	57.2	58.6	59.4	64.2	56.5
18.5	53	55.4	53.2	52.4	52.9	56.6	56.01	50.3
19	49.2	52.2	51.1	48.6	53.1	53.3	53.77	52.8
19.5	44.7	48.1	45.6	44.1	44.4	45.8	41.6	40.2
20	40	43.5	43	42.4	42.5	42.5	46	45.4
20.5	40	40.4	40.3	41	42	41	42.3	43
21	39.8	38	39.2	40.1	40	39.3	39	40.2
21.5	38	36.1	36.4	38.9	38.2	37.5	36.2	39.3
22	35.9	33	34.2	38	37.2	34	35	38.4
22.5	35.2	31.9	33	37.2	35.6	32.7	34.5	36.4
23	32	28	29	33.2	31.3	30.4	30	32.6
23.5	29	26.2	27.6	30	29.1	27.5	28.1	29
24	27	24.9	25.3	30	25.9	24.3	25	30.2

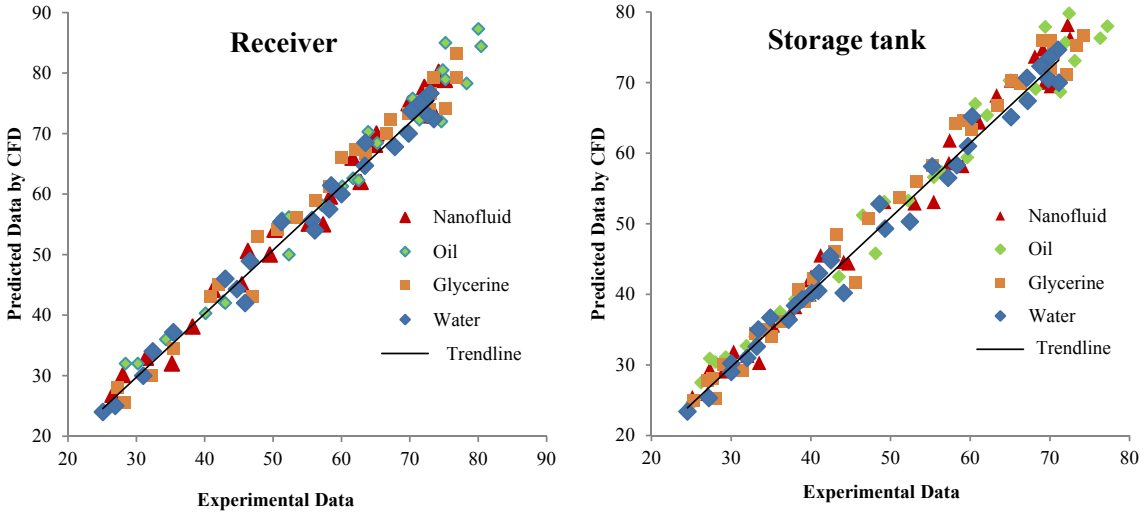

Fig. 17. Experimental outlet fluid temperature at receiver and storage tank outlet versus predicted data with different types of working fluids.

et al., 2016; Ghadirijafarbeigloo et al., 2014).

To validate the data obtained from CFD analysis method, the obtained simulation data were compared with experimental data considering the fluid temperature at outlet section of the storage tank showed in Fig. 17. It can be observed from the figure that the value of predicted temperature is almost higher than the data obtained by experimental condition (especially for hours the intensity of radiation is high). This is maybe due to variation of solar radiation, sun tracking method, environmental conditions which affected on the evaluation of outlet temperature of the receiver (Freitas, 2002). However the figure illustrated that selected CFD model is an appropriate method to predict the fluid thermal performance that flows through solar thermal system with different conditions with acceptable precision ($R^2 > 0.9532$). The other criterion for proving model accuracy is the relative error between CFD data (Pre) and test (Exp) data which changes between 2.8% and 5.9% for the receiver tube and 3.65%–7.92%. The results are acceptable considering similar thermal system (Ghasemi and Ranjbar, 2016; Khosravi and Malekan, 2018; Panchal Ramchandra and Bhosale, 2016).

The results of quality consideration factors of the dried samples (color, Shrinkage and rehydration ratio) showed that the effect of

Table 8
The quality characters of slices dried via solar cabinet dryer with different working fluids and in front of sun.

Quality character				
Drying mode	Working fluid	Color (ΔE)	Shrinkage (%)	RR
Solar cabinet dryer	Nanofluid	14.36 ± 0.72	82.23 ± 1.11	4.51 ± 0.16
	Oil	13.12 ± 0.66	80.45 ± 0.65	4.58 ± 0.15
	Glycerin	13.82 ± 0.89	82.26 ± 1.21	4.55 ± 0.12
	Water	15.54 ± 0.85	82.32 ± 1.32	4.34 ± 0.14
In front of sun	27.92 ± 0.82		85.24 ± 1.95	3.42 ± 0.21

drying condition on the quality of dried slices were not significant ($p > 0.05$). For all working fluids the results of quality factors were summarized in Table 8. The color is the first character that reflects a sensation to customer's eyes. In visual examination, the main attribute is attractive color of dried products for selecting and buying process. During the drying of agricultural products, drying temperature and drying time are two main parameters which significantly affected on the color quality of final dried samples (Samimi-Akhijahani et al., 2017, Tham et al., 2016). The calculated data shows that for the products dried in front of the sun lights due to direct exposure of samples to solar radiation and longer drying time, color changes are higher related to the other conditions. Moreover by the time browning of the samples occurred. The slices dried by system with oil as the working fluid has higher quality. This may be due to the short drying time compared to other conditions applied for drying process (Li et al., 2019; Elicin and Sacilik, 2005; Tiwari et al., 2016; Eltawil et al., 2018; Hossain and Bala, 2007, Thanaraj et al., 2007). The results of variation of shrinkage as the other quality parameter for all dried samples listed in Table 8. The results indicated that the samples which dried by water (as working fluid) due to the higher thermal capacity the temperature of fluid in the tank and the drying temperature inside the cabinet is lower. The drying temperature after sunset because of the heat capacity of water is higher than other parts of the system. The drying time of samples increased thus this increases the shrinkage of dried slices. Same results were recorded during drying process of apple (Lingayat et al., 2020; Yuan et al., 2019; Segura-Ponce et al., 2019; Schultz et al., 2007). Typically rehydration ratio indicated the changes of physicochemical properties of samples dried by different methods (Arabhosseini et al., 2019) and affected by various parameters including drying conditions, sample composition and microstructure, drying temperature and time. The difference between rehydration ratio (RR) of apple slices dried via different working fluids is not significant ($P > 0.05$). However for the slices dried by sun (direct condition) it was lower. When the samples dried with the method that takes longer time for drying of the samples, the structure and cells of slices destructed, the pores among the cells removed thus more time need to get back to initial matter content (Motahayyer et al., 2018; Zhu and Wenjing, 2010; Zhu and Pan, 2009; Sacilik and Elicin, 2006). Other studies reported the results which are in a good agreement with the present work results (Doymaz, 2010, Samimi-Akhijahani and Arabhosseini, 2018; Iranmanesh et al., 2020). According to the quality considerations of apple slices dried by other drying methods (Yuan et al., 2019; Djekic et al., 2018; Zhu et al., 2010; Zhu and Pan, 2009; Sacilik and Elicin, 2006; Fernandez et al., 2005), it is indicated that using different working fluid has no undesirable effect. Thus by considering the quality and economical factors, it can be stated that the cabinet solar dryer with PTSC and oil as working fluid assisted with phase change material could be a cheap and optimized way applied to dry wet biological products.

To illustrate the effect of using different working fluids on drying of apple slices some pictures of dried samples depicted in Fig. 18. It can be indicated that for the solar PTSC dryer with the air flow rate of 0.025 kg/s the quality of apple slices and the shape are promoted related to the slices dried in front of the sun.

4. Conclusion

An experimental and numerical study was performed to analysis thermal behavior and thermal efficiency of PTSC with different fluids. Moreover thermal behavior, fluid flow and temperature distribution of receiver during the experimental days was simulated using CFD. Four types of working fluids including water, glycerin, engine oil (SAE 10w40) and nanofluid (Al_2O_3 4%) were flows in the solar system using a hydraulic pump with flow rate of 4.2 l/min. To make the nano-fluid two step method (mechanical and ultrasonic mixing) was used. The vision test indicated that over the time there is no significant change in the mixture. Moreover, phase change material was placed inside the storage tank to increase the performance of the system. The results illustrated that the higher fluid temperature in the storage tank using nanofuid, engine oil, glycerine and water was 83.8, 88.2, 85.6 and 79.2 °C, respectively. Also, input thermal energy to solar dryer for mentioned fluids was 17.36 MJ, 18.46 MJ, 17.76 MJ and 16.80 MJ, respectively. Due to the nanoparticles, heat transfer coefficient of working fluid increased. Therefore thermal efficiency of solar collector connected to the dryer increased. Hourly thermal efficiency of PTSC showed that the amount of collector efficiency for the system with nanofluid, oil and glycerin is higher than water and it estimated about 5.83%, 9.27% and 7.67%. The collector efficiency with different working fluids obtained about 69.9%, 73.4%, 71.9% and 63.8% for nanofluid, oil, glycerine and water, respectively. The overall input thermal energy for nanofluid, engine oil, glycerine and water was about 42.92%, 46.65%, 43.95% and 39.11%. The drying kinetics of apple slices for all working fluid illustrated that the time consumed for drying process varies with different working fluids. Moreover, the drying rate increases with increasing solar radiation and then decreases. CFD simulation of the collector and the comparison of predicted data and test data implied that there is a good agreement (R^2 higher than 0.95). The quality consideration (color, shrinkage and rehydration ratio) of the dried product implied that using different nanofluid with PCM during the drying process improved the quality of the samples compared to the open sun drying mode. The research can be

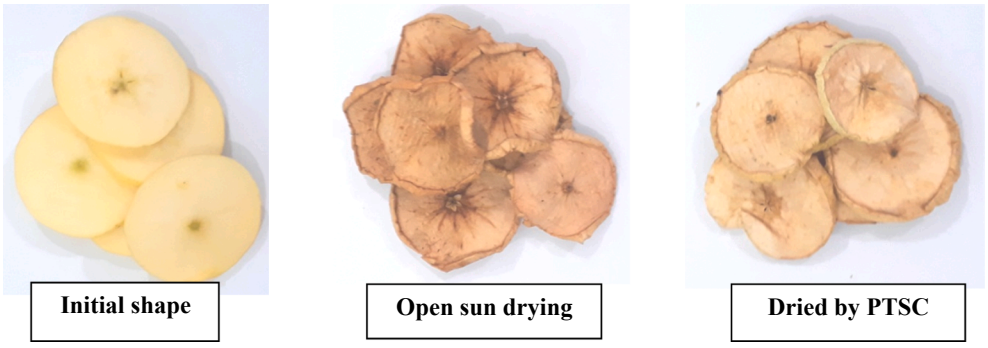

Fig. 18. Color and shape differences of dried apple slices: fresh sample, dried in front of sun and dried by PTSC.

used as the efficient and cheap method to get the higher thermal energy from the solar collectors to dry agricultural products. Using air recycling system with desiccant wheel could be the other way to improve the performance of the collector and dryer.

Declaration of Competing Interest

The authors declare that they have no known competing financial interests or personal relationships that could have appeared to influence the work reported in this paper.

Acknowledgements

Hereby the authors are gratefully to financial support by University of Kurdistan, Sanandaj, Iran for M.Sc thesis (No. 1529993).

References

Abbood, M.H., Mohammed, M.M., 2019. Experimental and theoretical investigation to generate steam by parabolic trough solar collector with using different heat transfer fluids. Int. J. Mech. Mechatron. Eng. 18 (6), 11–22.
Aghbashlo, M., Kianmehr, M.H., Samimi-Akhijahani, H., 2008. Influence of drying conditions on the effective moisture diffusivity, energy of activation and energy consumption during the thin-layer drying of beriberi fruit (Berberidaceae). Energy Convers. Manage. 49, 2865–2871.
Al-Abidi, A.A., Bin Mat, S., Sopian, K., Sulaiman, M.Y., Mohammed, A.T., 2013. CFD applications for latent heat thermal energy storage: a review. Renew. Sustain. Energy Rev. 20, 353–363.
Allouche, Y., Varga, S., Bouden, C., Oliveira, A.C., 2016. Validation of a CFD model for the simulation of heat transfer in a tubes-in-tank PCM storage unit. Renew. Energy 89, 371–379.
Ambekar, A.S., Sivakumar, R., Anantharaman, N., Vivekenandan, M., 2016. CFD simulation study of shell and tube heat exchangers with different baffle segment configurations. Appl. Therm. Eng. 108, 999–1007.
Amjad, W., Munir, A., Esper, A., Hensel, O., 2015. Spatial homogeneity of drying in a batch type food dryer with diagonal air flow design. J. Food Eng. 144, 148–155.
Arabhosseini, A., Samimi-Akhijahani, H., Motahayyer, M., 2019. Increasing the energy and exergy efficiencies of a collector using porous and recycling system. Renew. Energy 132, 308–325.
Babu, C.R., Gugulothu, S.K., 2015. CFD analysis of heat transfer enhancement by using passive technique in heat exchanger. Int. J. Rece. Adv. Mech. Eng. (IJMECH) 4 (3).
Bellos, E., Tzivanidis, C., 2017. Parametric investigation of nanofuids utilization in parabolic trough collectors. Therm. Sci. Eng. Prog. 2, 71–79.
Bellos, E., Tzivanidis, C., Antonopoulos, K.A., Gkinis, G., 2016a. Thermal enhancement of solar parabolic trough collectors by using nanofluids and converging-diverging absorber tube. Renew. Energy 94, 213–222.
Bellos, E., Tzivanidis, C., Antonopoulos, K.A., Daniil, I., 2016b. The use of gas working fluids in parabolic trough collectors – an energetic and exergetic analysis. Appl. Therm. Eng. 109 (A), 1–14.
Bellos, E., Daniil, I., Tzivanidis, C., 2018. Multiple cylindrical inserts for parabolic trough solar collector. Appl. Therm. Eng. 143, 80–89.
Boulard, T., Wang, S., 2002. Experimental and numerical studies on the heterogeneity of crop transpiration in a plastic tunnel. Comput. Electron. Agric. 34, 173–190.
Brandl, D., Mach, T., Kaltenecker, P., Sterrer, R., Neururer, C., Treberspurg, M., Hochenauer, C., 2015. CFD assessment of a solar honeycomb (SHC) facade element with integrated PV cells. Sol. Energy 118, 155–175.
Chon, C.H., Kihm, K.D., Lee, S.P., Choi, S.U.S., 2005. Empirical correlation finding the role of temperature and particle size for nanofluid (Al_2O_3) thermal conductivity enhancement. J. Phys. 87, 1–3.
Daniel, P., Joshi, Y., Das, A.K., 2011. Numerical investigation of parabolic trough receiver performance with outer vacuum shell. Sol. Energy 85 (9), 1910–1914.
DanlamiMusa, S., Zhonghua, T., Ibrahim, A., Habib, M., 2018. China's energy status: A critical look at fossils and renewable options. Renew Sustain Energy Rev. 81 (2), 2281–2290.
Darabi, H., Zomorodian, A., Akbari, M.H., Lorestani, A.N., 2013. Design a cabinet dryer with two geometric configurations using CFD. J. Food Sci. Tech. 52 (1), 359–366.
Darvishi, H., Zarein, M., Farhudi, Z., 2016. Energetic and exergetic performance analysis and modeling of drying kinetics of kiwi slices. J. Food. Sci. Technol. 53 (5), 2317–2333.
Demir, M.E., Dincer, I., 2017. Development of a hybrid solar thermal system with TEG and PEM electrolyzer for hydrogen and power production. Int. J. Hydrogen Energy 42 (51), 30044–30056.
Demissie, P., Gebrehiwot, M., Vanierschot, M., 2019. On the comparison between computational fluid dynamics (CFD) and lumped capacitance modeling for the simulation of transient heat transfer in solar dryers. Sol. Energy 184, 417–425.
Djekic, I., Tomic, N., Bourdoux, S., Spilimbergo, S., Smigic, N., Udovicki, B., Hofland, G., Devlieghere, F., Rajkovic, A., 2018. Comparison of three types of drying (supercritical CO2, air and freeze) on the quality of dried apple – Quality index approach. LWT 94, 64–72.
Doymaz, I., 2010. Effect of citric acid and blanching pre-treatments on drying and rehydration of Amasya red apples. Food Bioprod. Process. 88, 124–132.
Duffie, J.A., Beckman, W.A., 2013. Solar Engineering of Thermal Processes, fourth ed. Wiley, New York.
Dutil, Y., Rousse, D.R., Salah, N.B., Lassue, S., Zalewski, L., 2011. A review on phase change materials: mathematical modeling and simulations. Renew. Sustain. Energy Rev. 15, 112–130.
Elicin, A.K., Sacilik, K., 2005. An experimental study for solar tunnel drying of apple. Trim Bilimleri Deregisi 11 (2), 207–211.
Eltawil, M.A., Azama, M.M., Alghannam, A.O., 2018. Solar PV powered mixed-mode tunnel dryer for drying potato chips, Renew. Energy 116, 594–605.
Evin, A., 2011. Thin layer drying kinetics of *Gundelia Tournefortii L*. Food Bioprod, Process. 90 (2), 323–332.
Fernandez, L., Castillero, C., Aguilera, J.M., 2005. An application of image analysis to dehydration of apple discs. J. Food Eng. 67 (1–2), 185–193.
Gertzos, K.P., Caouris, Y.G., 2007. Experimental and computational study of the developed flow field in a flat plate integrated collector storage (ICS) solar device with recirculation. Exp. Therm. Fluid Sci. 31 (8), 1133–1145.
Ghadirijafarbeigloo, S., Zamzamian, A., Yaghoubi, M., 2014. 3-D numerical simulation of heat transfer and turbulent flow in a receiver tube of solar parabolic trough concentrator with louvered twisted-tape inserts. Energy Proc. 49, 373–380.
Ghasemi, S.E., Ranjbar, A.A., Ramiar, A., 2013. Three-dimensional numerical analysis of heat transfer characteristics of solar parabolic collector with two segmental rings. J. Math. Comput. Sci. 7, 89–100.
Ghasemi, S.E., Ranjbar, A., 2015. Effect of nanoparticles in working fluid on thermal performance of solar parabolic trough collector. J. Mol. Liq. 89, 368–375.
Ghasemi, S.E., Ranjbar, A.A., 2016. Thermal performance analysis of solar parabolic trough collector using nanofluid as working fluid: a CFD modelling study. J. Mol. Liq. 222, 159–166.
Goyal, R.K., Tiwari, G.N., Garg, H.P., 1998. Effect of thermal storage on the performance of an air collector: a periodic analysis. Energy Convers. Manage. 39, 193–202.
Gunjo, D.G., Mahanta, P., Robi, P.S., 2017. Exergy and energy analysis of a novel type solar collector under steady state condition: Experimental and CFD analysis. Renew. Energy. 114, 655–669.
Habibi, H., Zoghi, M., Chitsaz, A., Javaherdeh, K., Ayazpour, M., 2019. Thermo-economic performance comparison of two confgurations of combined steam and organic Rankine cycle with steam Rankine cycle driven by Al_2O_3-therminol VP-1 based PTSC. Sol. Energy 180, 116–132.
Hachicha, A.A., Rodriguez, I., Lehmkuhl, O., Oliva, A., 2014. On the CFD & HT of the flow around a parabolic trough solar collector under real working conditions. Energy Proc. 49, 1379–1390.
Haller, M.Y., Cruichshank, C.A., Streicher, W., Harrison, S.J., Andersen, E., Furbo, S., 2009. Methods to determine stratification efficiency of thermal energy storage processes –Review of theoretical comparison. Sol. Energy 83 (10), 1847–1860.
Holman, J.P., 2002. Heat Transfer, tenth edition. Published by Mc-Grow Hill, Southern Methodist University, New York.
Hossain, M.A., Bala, B.K., 2007. Drying of hot chilli using solar tunnel drier. Sol. Energy 81 (1), 85–92.
Hosseini, M.J., Ranjbar, A.A., Sedighi, K., Rahimi, M., 2012. A combined experimental and computational study on the melting behavior of a medium temperature phase change storage material inside shell and tube heat exchanger. Int. Commun. Heat Mass Transf. 39, 1416–1424.
Hung, T.C., Huaung, T.J., Lee, D.S., Lin, C.H., Pei, B.S., Li, Z.Y., 2017. Numerical analysis and experimental validation of heat transfer characteristic for flat-plate solar air collector. Appl. Therm. Eng. 111 (25), 1025–1038.
Iranmanesh, M., Akhijahani, H.S., Jahromi, M.S.B., 2020. CFD modeling and evaluation the performance of a solar cabinet dryer equipped with evacuated tube solar collector and thermal storage system. Renew. Energy 145, 1192–1213.
Jaramillo, O., Borunda, M., Velazquez-Lucho, K., Robles, M., 2016. Parabolic trough solar collector for low enthalpy processes: An analysis of the efficiency enhancement by using twisted tape inserts. Renew. Energy 93, 125–141.
Javadi-Yanblagh, D., Toori-Bidgoli, H., 2015. Comparative study of the production of dried apples by solar dryer and other drying methods. Int. Conf. Environ, Sci. Energy Technol. (CESET).
Kalogirou, S., 2009. Environmental Characteristics – Chapter two. Sol. Energy Eng. (Process. Syst.) 49–120.
Kalogirou, S.A., 2012. A detailed thermal model of a parabolic trough collector receiver. Energy 48 (1), 298–306.
Kaloudis, E., Papanicolaou, E., Belessiotis, V., 2016. Numerical simulations of a parabolic trough solar collector with nanofluid using a two-phase model. Renew. Energy 97, 218–229.
Karmare, S.V., Tikekar, A.N., 2010. Analysis of fluid flow and heat transfer in a rib grit roughened surface solar air heater using CFD. Sol. Energy 84 (3), 409–417.
Kasaeian, A., Daviran, S., Azarian, R.D., Rashidi, A., 2015. Performance evaluation and nanofluid using capability study of a solar parabolic trough collector. Energy Convers. Manage. 89, 368–375.
Kaya, M., Etem-Gurel, A., Agbulut, U., Ceylan, I., Celik, S., Ergun, A., Acar, B., 2019. Performance analysis of using CuO-Methanol nanofluid in a hybrid system with concentrated air collector and vacuum tube heat pipe. Energy Convers. Manage. 199 (1), 111936.
Khanafer, K., Vafaei, K., 2011. A critical synthesis of thermophysical characteristics of nanofluids. Int. J. Heat Mass Transf. 54, 4410–4428.
Khosravi, A., Malekan, M., 2018. Effect of magnetic field on heat transfer coefficient of Fe_3O_4-water ferrofluid using artificial intelligence and CFD simulation. Eur. Phys. J. Plus 134 (88), 1–21.
Khosravi, A., Malekan, M., Assad, M.E.h., 2019. Numerical analysis of magnetic field effects on the heat transfer enhancement in ferrofluids for a parabolic trough solar

collector. Renew. Energy 134, 54–63.
Krawczyk, P., Badyda, K., 2011. Two-dimensional CFD modeling of the heat and mass transfer process during sewage sludge drying in a solar dryer. Arch. Thermo-dyn. 32, 3–16.
Kumaresan, G., Sridhar, R., Velraj, R., 2012. Performance studies of a solar parabolic trough collector with a thermal energy storage system. Energy 47, 395–402.
Lacroix, M., 1993. Numerical simulation of a shell-and-tube latent heat thermal energy storage unit. Sol. Energy 50 (4), 357–367.
Li, X., Wu, X., Bi, J., Liu, X., Li, X., Guo, G., 2019. Polyphenols accumulation effects on surface color variation in apple slices hot air drying process. LWT 108, 421–428.
Liangdong, M., Zhen, L., Jili, Z., Ruobing, L., 2010. Thermal performance analysis of the glass evacuated tube solar collector with U-tube. Build. Environ. 45 (9), 1050–1967.
Lingayat, A., Chandramohan, V.P., Raju, V.R.K., Kumar, A., 2020. Development of in-direct type solar dryer and experiments for estimation of drying parameters of apple and watermelon. Therm. Sci. Eng. Prog. 16, 100477.
Lobon, D.H., Valenzuela, L., Baglietto, E., 2014. Modeling the dynamics of the multiphase fluid in the parabolic-trough solar steam generating systems. Energy Convers. Manage. 78, 393–404.
Malekjani, N., Jafari, S.M., 2018. Simulation of food drying processes by Computational Fluid Dynamics (CFD); recent advances and approaches. Trend. Food Sci. Technol. 78, 206–223.
Malvandi, A., Heysiattalab, S., Ganji, D.D., 2016. Effects of magnetic field strength and direction on anisotropic thermal conductivity of ferrofluids (magnetic nano-fluids) at filmwise condensation over a vertical cylinder. Adv. Powder Technol. 27, 1539–1546.
Manikandan, K., Kumaresan, G., Velraj, R., Iniyan, S., 2012. Parametric study of solar parabolic trough collector system, Asian. J. Appl. Sci. 5, 384–393.
Marrakchi, Salma, Leemrani, Zouhir, Asselman, Hassan, Aoukili, Abdeslam, Asselman, Adel, 2018. Temperature distribution analysis of parabolic trough solar collector using CFD. Proc. Manuf. 22, 773–779. https://linkinghub.elsevier.com/retrieve/pii/S2351978918304062https://doi.org/10.1016/j.promfg.2018.03.110.
Mohammad Zadeh, P., Sokhansefat, T., Kasaeian, A.B., Kowsary, F., Akbarzadeh, A., 2015. Hybrid optimization algorithm for thermal analysis in a solar parabolic trough collector based on nanofluid. Energy 82, 857–864.
Moloodpoor, M., Mortazavi, A., Ozbalta, N., 2019. Thermal analysis of parabolic trough collectors via a swarm intelligence optimizer. Sol. Energy 181, 264–275.
Moreira, R., Figueiredo, A., Sereno, A., 2000. Shrinkage of apple disks during drying by warm air convection and freeze drying. Drying Technol. 18 (1–2), 279–1194.
Motahayyer, M., Arabhosseini, A., Samimi-Akhijahani, H., Khashechi, M., 2018. Application of computational fluid dynamics in optimization design of absorber plate of solar dryer. Iran. J. Biosys. Eng. 49 (2), 285–294 (in Persian).
Motevali, A., 2013. Design and Evaluation of a Parabolic Sun Tracking Collector for Drying of Mint. [Ph.D. Thesis]. Tarbiat Modares University, Tehran, Iran.
Munoz, J., Abanades, A., 2011. Analysis of internal helically finned tubes for parabolic trough design by CFD tools. Appl. Energy 88, 4139–4149.
Mwesigye, A., Huan, Z., Meyer, J.P., 2015. Thermodynamic optimisation of the performance of a parabolic trough receiver using synthetic oil–Al_2O_3 nanofluid. Appl. Energy 156, 398–412.
Mwesigye, A., Huan, Z., 2015. Thermal and thermodynamic performance of a parabolic trough receiver with Syltherm800-Al_2O_3 nanofluid as the heat transfer fluid. Energy Proc. 75, 394–402.
Neha, J., 2012. Comparative study of parabolic trough collector and solar power tower technology. Int. J. Sci. Res. Rev. 1 (3), 64–74.
Othman, M.F., Adam, A., Najafi, G., Mamat, R., 2017. Green fuel as alternative fuel for diesel engine: A review. Renew. Sustain. Energy Rev. 80, 694–709.
Panchal Ramchandra, H., Bhosale, S.K., 2016. The CFD analysis of solar parabolic trough system with reflectors. Int. J. Curr. Eng. Technol. 5, 431–435.
Romano, G., Kocsis, L., Farkas, I., 2009. Analysis of energy and environmental parameters during solar cabinet drying of apple and carrot. Dry. Technol. 27 (4), 574–579.
Ross, S.A., Westerfield, R.W., Jaffe, J., 2007. Modern Financial Management, eight ed. McGraw Hill Higher Education, pp. 926.
Ruvinda, K.K.D.L., Suraweera, S.K.K., Jayaweera, H.H.E., Ranasinghe, O.K., Ariyaratne, T.R., 2011. Construction and evaluation of a drying chamber powered by parabolic trough solar concentrator for drying of agricultural and other materials. Proc. Tech. Sess. 27, 114–122.
Shih, T.H., Liou, W.W., Shabbir, A., Yang, Z., Zhu, J., 1995. A new k-ϵ eddy viscosity model for high reynolds number turbulent flows. Comput Fluids. 24 (3), 227–238.
Sacilik, K., Elicin, A.K., 2006. The thin layer characteristics of organic apple slices. J. Food Eng. 73, 281–289.
Samimi-Akhijahani, H., Arabhosseini, A., Kianmehr, M.H., 2016. Effective moisture diffusivity during hot air solar drying of tomato slices. Res. Agric. Eng. 62, 15–23.
Samimi-Akhijahani, H., Arabhosseini, A., Kianmehr, M.H., 2017. Comparative quality assessment of different drying procedures for plum fruits (Prunus domestica L.). Czech J. Food Eng. 35, 449–455.
Samimi-Akhijahani, H., Arabhosseini, A., 2018. Accelerating drying process of tomato slices in a PV-assisted solar dryer using a sun tracking system. Renew. Energy 123, 428–438.
Schultz, E.L., Mazzuco, M.M., Machado, R.A.F., Bolzan, A., Quadri, M.B., Quadri, M.G.N., 2007. Effect of pre-treatments on drying, density and shrinkage of apple slices. J. Food Eng. 78 (3), 1103–1110.
Segura-Ponce, L.A., Soto-Pardo, V.A., Guzmán-Meza, M.F., 2019. Characterization of apples (Granny Smith) dried in industrial equipment and the relationship with drying mechanisms. Food Struct. 21, 100119.
Shanmugam, V., Natarajan, E., 2007. Experimental study of regenerative desiccant integrated solar dryer with and without reflective mirror. Appl. Therm. Eng. 27, 1543–1551.
Sharafeldin, M.A., Grof, G., 2018. Evacuated tube solar collector performance using CeO2/water nanofluid. J. Cleane. Produc. 185, 347–356.
Singh, A.P., Singh, O.P., 2018. Performance enhancement of a curved *solar* air heater using *CFD*. Sol. Energy. 174 (1), 556–569.
Sokhansefat, T., Kasaeian, A.B., Kowsary, F., 2014. Heat transfer enhancement in parabolic trough collector tube using Al_2O_3/synthetic oil nanofluid. Renew. Sustain. Energy Rev. 33, 636–644.
Tay, N.H.S., Bruno, F., Belusko, M., 2012a. Experimental validation of a CFD model for tubes in a phase change thermal energy storage system. Int. J. Heat Mass Transfer 55, 574–585.
Tay, N.H.S., Belusko, M., Bruno, F., 2012b. Experimental investigation of tubes in a phase change thermal energy storage system. Appl. Energy 90 (1), 288–297.
Tiwari, S., Tiwari, G.N., Al-Helal, I.M., 2016. Performance analysis of photo-voltaic–thermal (PVT) mixed mode greenhouse solar dryer. Sol. Energy 133, 421–428.
Thanaraj, T., Dharmasena, N.D.A., Samarajeewa, U., 2007. Comparison of quality and yield of copra processed in CRI improved kiln drying and sun drying. J. Food Eng. 78 (4), 1446–1451.
Tarigan, E., 2018. Mathematical modeling and simulation of a solar agricultural dryer with back-up biomass burner and thermal storage. Case Stud. Therm. Eng. 12, 149–165.
Tham, T.C., Ng, M.X., Gan, S.H., Chua, L.S., Aziz, R., Abdullah, L.C., Ong, S.P., Chin, N.L., Law, C.L., 2016. Impacts of different drying strategies on drying characteristics, the retention of bio-active ingredient and colour changes of dried Roselle. Chin. J. Chem. Eng. 26 (2), 303–316.
Toghyani, S., Baniasadi, E., Afshari, E., 2016. Thermodynamic analysis and optimization of an integrated Rankine power cycle and nano-fuid based parabolic trough solar collector. Energy Convers. Manage. 121, 93–104.
Tong, Y., Lee, H., Kang, W., Cho, H., 2019. Energy and exergy comparison of a flat-plate solar collector using water, Al_2O_3 nanofluid, and CuO nanofluid. Appl. Therm. Eng. 159, 113959.
Trostle, R., 2008. Global agricultural supply and demand: Factor contributing to the recent increase in food commodity price. Outlook report No. WRS-0801. Economic research service, U.S. Department of Agriculture.
Trp, A., Lenic, K., Frankovic, B., 2006. Analysis of the influence of operating conditions and geometric parameters on heat transfer in water-paraffin shell-and-tube latent thermal energy storage unit. Appl. Therm. Eng. 26, 1830–1839.
Tzirtzilakis, E., Kafoussias, N., 2010. Three-dimensional magnetic fluid boundary layer flow over a linearly stretching sheet. J. Heat Tran. 132 (1), 011702.
Vieira, M.G.A., Estrella, L., Rocha, S.C.S., 2007. Energy efficiency and drying kinetics of recycled paper pulp. Dry. Technol. 25, 1639–1648.
Wang, Y., Xu, J., Liu, Q., Chen, Y., Liu, H., 2016. Performance analysis of a parabolic trough solar collector using Al_2O_3/synthetic oil nanofluid. Appl. Therm. Eng. 107, 469–478.
Yadav, A., Kumar, M., Balram, 2013. Experimental study and analysis of parabolic trough collector with various reflectors. Int. J. Math. Comput. Physic. Quant. Eng. 7 (12), 1157–1161.
Yaghoubi, M., Ahmadi, F., Bandehee, M., 2013. Analysis of heat losses of absorber tubes of parabolic through collector of Shiraz (Iran) solar power plant. J. Clean. Energy Technol. 1 (1), 33–37.
Xiaohong, G., Bin, L., Yongxian, G., Xiugan, Y., 2011. Two-dimensional transient thermal analysis of PCM canister of a heat pipe receiver under microgravity. Appl. Therm. Eng. 31, 735–741.
Yashavant, J., Daniel, P., Das, A.K., 2011. Numerical investigation of parabolic trough receiver with outer vacuum shell. Sol. Energy 85, 1910–1914.
Yilmaz, I.H., Soylemez, M.S., 2014. Thermo-mathematical modeling of parabolic trough collector. Energy Convers. Manage. 88, 768–784.
Yuan, Y., Tan, L., Xu, Y., Yuan, Y., Dong, J., 2019. Numerical and experimental study on drying shrinkage-deformation of apple slices during process of heat-mass transfer. Int. J. Therm. Sci. 136, 539–548.
Zhai, Y., Li, L., Wang, J., Li, Z., 2019. Evaluation of surfactant on stability and thermal performance of Al_2O_3-ethylene glycol (EG) nanofluids. Powd. Technol. 343, 215–224.
Zhao, M., Liu, Z., Zhang, Q. 2009. Feasibility analysis of constructing parabolic trough solar thermal power plant in inner Mongolia of China. In: Proc. Asia - Pacific Power and Energy Engineering Conference, pp. 1–4.
Zheng, Z., Xu, Y., He, Y., 2016. Thermal analysis of a solar parabolic trough receiver tube with porous insert optimized by coupling genetic algorithm and CFD. Sci. China Tech. Sci. 59, 1475–1485.
Zhu, Y., Pan, Z., 2009. Processing and quality characteristics of apple slices under simultaneous infrared dry-blanching and dehydration with continuous heating. J. Food Eng. 90 (4), 441–452.
Zhu, T., Wenjing, Y., 2010. Numerical heat and transfer part B, Fundamental: Theoretical and numerical studies of non-continuum gas - phase heat conduction micro/nano devices. Taylor and Francis, pp. 203–226.
Zhu, Y., Pan, Z., McHugh, T.H., Barrett, D.M., 2010. Processing and quality characteristics of apple slices processed under simultaneous infrared dry-blanching and dehydration with intermittent heating. J. Food Eng. 97 (1), 8–16.
Freitas, C.J., 2002. The issue of numerical uncertainty. Appl. Math. Model. 26 (2), 237–248.